Magnesium (Mg/Ca, $\delta^{26}Mg$), boron (B/Ca, $\delta^{11}B$), and calcium (Ca^{2+}) geochemistry of *Arctica islandica* and *Crassostrea virginica* extrapallial fluid and shell under ocean acidification

Blanca Alvarez Caraveo[1,2], Maxence Guillermic[1,2,3], Alan Downey-Wall[4], Louise P. Cameron[4], Jill N. Sutton[5], John A. Higgins[6], Justin B. Ries[4], Katie Lotterhos[4], Robert A. Eagle[1,2]

[1]Atmospheric and Oceanic Sciences Department, University of California, Los Angeles, Math Sciences Building, 520 Portola Plaza, Los Angeles, CA 90095, USA
[2]Center for Diverse Leadership in Science, Institute of the Environment and Sustainability, University of California, Los Angeles, LaKretz Hall, 619 Charles E Young Dr E no. 300, Los Angeles, CA 90024, USA
[3]Earth, Planetary and Space Sciences, Department, University of California, Los Angeles, Los Angeles, CA 90095, USA
[4] Department of Marine and Environmental Sciences, Marine Science Center, Northeastern University, 430 Nahant Rd, Nahant, MA 01908, USA
[5] Université de Brest, UMR 6539 CNRS/UBO/IRD/Ifremer, LEMAR, IUEM, 29280, Plouzané, France
[6] Department of Geosciences, Princeton University, Guyot Hall, Princeton NJ 08544, USA

Correspondence to: Blanca Alvarez Caraveo (alvarezblanca@g.ucla.edu) and Robert Eagle (robeagle@ucla.edu)

Abstract. The geochemistry of biogenic carbonates has long been used as proxies to record changing seawater parameters. However, the effect of ocean acidification (OA) on seawater chemistry and organism physiology could impact isotopic signatures and how elements are incorporated into the shell. In this study, we investigated the geochemistry of three reservoirs important for biomineralization - seawater, the extrapallial fluid (EPF), and the shell - in two bivalve species, *Crassostrea virginica* and *Arctica islandica*. Additionally, we examined the effects of three ocean acidification conditions (ambient: 500 ppm CO_2, moderate: 900 ppm CO_2, and high: 2800 ppm CO_2) on the geochemistry of the same three reservoirs for *C. virginica*. We present data on calcification rates, EPF pH, measured elemental ratios (Mg/Ca, B/Ca), and isotopic signatures ($\delta^{26}Mg$, $\delta^{11}B$). In both species, comparisons of seawater and EPF Mg/Ca and B/Ca, Ca^{2+}, and $\delta^{26}Mg$ indicate that the EPF has a distinct composition that differs from seawater. Shell $\delta^{11}B$ did not faithfully record seawater pH and $\delta^{11}B$-calculated pH values were consistently higher than pH measurements of the EPF with microelectrodes, indicating that the shell $\delta^{11}B$ may reflect a localized environment within the entire EPF reservoir. In *C. virginica*, EPF Mg/Ca and B/Ca, as well as absolute concentrations of Mg^{2+}, B, and Ca^{2+}, were all significantly affected by ocean acidification, indicating that OA affects the physiological pathways regulating or storing these ions, an observation that complicates their use as proxies. Reduction in EPF Ca^{2+} may represent an additional mechanism underlying reduction in calcification in *C. virginica* in response to seawater acidification. The complexity of dynamics of EPF chemistry suggest boron proxies in these two

mollusc species are not straightforwardly related to seawater pH, but ocean acidification does lead to both a decrease in microelectrode pH and boron-isotope-based pH, potentially showing applicability of boron isotopes in recording physiological changes. Collectively, our findings show that bivalves have high physiological control over the internal calcifying fluid, which presents a challenge to using boron isotopes for reconstructing seawater pH.

1 Introduction

The elemental geochemistry of marine biogenic carbonate shells is widely used to track and reconstruct environmental change (e.g. Broecker and Peng, 1982; Elderfield et al., 2006). The incorporation of elements within the skeleton of marine calcifiers has been shown to be correlated with different environmental parameters, such as temperature (Dunbar et al., 1994; Alibert and McCulloch 1997) and pH (e.g. Hemming and Hanson, 1992; Hönisch et al., 2004; McCulloch et al., 2018). However, elemental and isotopic signatures of biogenic carbonate deviate from inorganic carbonate grown under the same conditions, complicating the use and interpretation of these theoretical models for paleo-reconstructions (e.g. Urey, 1951; Craig, 1953; Weiner and Dove, 2003). "Vital effects" are the physiological processes that alter the geochemistry of biominerals and consequently offset the environmental signal incorporated in biogenic carbonates, which includes the different biomineralization strategies that can modify the chemistry of the calcification fluid (Urey, 1951; Weiner and Dove, 2003). For organisms to calcify, a semi-isolated calcification space will be, to varying degrees, separated from seawater for supersaturation to be achieved in support of calcification (Weiner and Dove, 2003). The geochemistry of the calcification fluid can be altered due to isolation from the parent fluid as well as the modulation of the calcification fluid chemistry via methods of passive or active ion transport to the site of calcification (Weiner and Dove 2003; McCulloch et al., 2017; Sutton et al., 2018; Liu et al., 2020). A mechanistic understanding of such vital effects is desirable for the accurate interpretation of geochemical proxies preserved in the shells of these organisms.

Bivalve extrapallial fluid (EPF) is an internal fluid reservoir physically semi-separated from seawater that circulates in the pallial cavity, between the mantle organ and shell (Wilbur and Saleuddin, 1983). Seawater enters the pallial cavity when valves are open, then the internal hemolymph fluid circulates within the organs of the mollusc and finally can also be transported across the mantle to the EPF (Zhao et al., 2018). Bivalve mollusc shell calcification is thought to occur at the interface of the EPF and growing shell where the ions for calcification interact with organic matrices, such as polypeptide molecules and proteins within the EPF that act as a scaffolding template for nucleation and are important in the calcification process (e.g. Crenshaw, 1972; Wilbur and Bernhardt, 1984; Addadi, 2006; Checa 2018). Unlike the calcifying fluid reservoirs in most organisms, bivalve EPF has a large enough volume that it can be directly sampled, allowing for direct measurements of the reservoir to compare with seawater geochemistry and elucidate *in situ* changes in EPF chemistry. A foundational study by Crenshaw (1972) found that, in three mollusc species, the EPF calcification fluid had a different chemical composition and pH from seawater and hemolymph fluid (Crenshaw et al., 1972). A previous study on the king scallop, *Pecten maximus*, by Cameron et al. (2019) showed that EPF pH was lower than seawater and also depended on

seawater pCO_2 and temperature. Additionally, Ramesh et al., (2017) used a microelectrode approach to show that pH and $[CO_3^{2-}]$ were elevated proximal to the growing shell in larval *Mytilus edulis* shells. This result using microelectrode suggests a potential difference in pH between the bulk EPF and the pH close to the site of calcification. In the quahog *Arctica islandica*, Stemmer et al. (2019) reported synchronous short-term fluctuations in EPF Ca^{2+} and the pH at the outer mantle epithelium surface, providing further support that the extrapallial fluid of molluscs is a discrete fluid under biological control. Understanding the elemental composition and isotope signatures of mollusc internal fluid reservoirs, mechanisms of calcification, and ion transport to the site of calcification is critical to understanding these vital effects. It may also give insight into the sensitivity of bivalves to pCO_2-induced ocean acidification, a major environmental challenge for bivalves, which are typically amongst the more sensitive group of marine calcifier species to acidification (Ries et al., 2009; Kroecker et al., 2011; Gazeau et al., 2013; Stewart-Sinclair et al., 2020).

Molluscs have long been recognized as valuable archives for climate reconstructions, given their annual resolution growth bands, long lifespans, and wide geographic distributions (Gibson et al., 2001; Peharda et al., 2021). Several different elemental systems like boron (B) and magnesium (Mg^{2+}) have the potential to give valuable information about the seawater bivalves precipitate their shells in or even in internal calcification fluid they precipitate their shells from. For example, shell B/Ca has been shown to be correlated to EPF pH in bivalves such as *M. edulis* (Heinemann et al., 2012) and *Mercenaria mercenaria* (Ulrich et al., 2021), and can potentially be useful in understanding the internal carbonate chemistry within the calcification fluid. Shell $\delta^{11}B$ is used as a proxy for seawater pH in foraminifera (Foster and Rae, 2016) and calcification fluid pH in corals (McCulloch et al., 2017; Eagle et al., 2022), but seems to be offset from theoretical pH calculations in bivalves like *M. edulis* (e.g. Heinemann et al., 2012; Liu et al., 2020), *M. mercenaria* (Liu et al., 2020), and *Crassostrea virginica* (Liu et al., 2020). Shell Mg/Ca is used as a temperature proxy in bivalves (Wanamaker et al., 2008; Schöne et al., 2011), however molluscs can regulate and actively exclude Mg^{2+} from their shells (e.g. Lorens and Bender, 1977; Planchon et al., 2013), showing that biological regulation of the internal fluids for shell formation can have a strong influence on Mg-based geochemical proxies. Furthermore, Mg isotope analyses can potentially inform the Mg^{2+} transport process in molluscs. Although few Mg isotopic studies on molluscs have been done, a study by Planchon et al. (2013) investigated the $\delta^{26}Mg$ of *Ruditapes philippinarum* tissues, shell, and EPF and found that seawater and EPF Mg isotopic signatures were similar, suggesting that seawater is the source of Mg^{2+} ions within the EPF. Additionally, they found that Mg isotopic signatures of some specimens deviated from inorganically precipitated aragonite, suggesting an ability to physiologically alter or regulate Mg^{2+} within the EPF (Planchon et al., 2013).

Marine calcifiers are thought to be particularly sensitive to ocean acidification because of lowered saturation state of calcite ($\Omega_{calcite}$) and availability of carbonate ions they need to precipitate their shells (Orr et al., 2005). However, marine calcifiers can exhibit extremely different calcification responses to ocean acidification (e.g. Ries et al., 2011; Kroeker et al., 2013). Bivalves show similar variable responses to ocean acidification (Gazeau et al., 2013). A study conducted by Waldbusser et al. (2015) found that juvenile *Crassostrea gigas* and *Mytilus galloprovincialis* had developmental and growth sensitivities to decreasing seawater $\Omega_{calcite}$. Furthermore, a study by Fitzer et al. (2016) found that *M. edulis* shell

crystallography was affected by ocean acidification, compromising the organism's shell. Additionally, studies have found that exposure to ocean acidification conditions could affect trace element uptake in bivalve shells (Norrie et al., 2018; Zhao et al., 2020). The effects of ocean acidification on bivalve shell geochemistry is of particular consequence for paleoclimate reconstructions due to primary or secondary effects such as calcification or physiological impairment. (e.g. Michaelidis et al., 2005; Waldbusser et al., 2015; Norrie et al., 2018; Zhao et al., 2020).

Few taxa have been studied using combined geochemical tracer work to determine the chemistry of calcification fluid pools and sources of ions to the calcification front. To date, one study has investigated the B/Ca and $\delta^{11}B$ of shell and EPF of the bivalve *M. edulis* (Heinemann et al., 2012). Mollusc extrapallial fluid is an attractive target to investigate geochemical vital effects because not only can it be probed with electrodes, but it can also be extracted and analyzed. In this study, we investigate the $\delta^{11}B$, B/Ca, $\delta^{26}Mg$, and Mg/Ca of extracted EPF and aragonite shell of the quahog, *A. islandica*, and the calcite shell of the eastern oyster, C *virginica*. This allows for the investigation of the tripartite fractionation between seawater, EPF, and shell. Individuals were kept in controlled laboratory experiments, with EPF pH determined with microelectrodes, and other physiological parameters, such as calcification rate, determined by conventional methods (Downey-Wall et al., 2020). Additionally, in order to examine if elemental ratios and isotopic signatures can be impacted under ocean acidification, specimens of *C. virginica* were also cultured in three different treatments of pCO_2: ambient, moderate and high ocean acidification conditions. Geochemical analysis of the seawater, shell, and EPF thereby allow novel insights into the transport of ions from seawater to the EPF, and the fractionation of isotopes and elements between the EPF and shell for both species. Additionally, how the same analyses can change for *C. virginica* under acidified conditions.

2 Materials and Methods

2.1 Experimental Conditions

Adult *A. islandica* specimens were collected from Beals Island, Maine, USA (44° 31 '11”N, 67° 36' 54”W) in March 2018, transferred to Northeastern University’s Marine Science Center, and maintained in the lab until March 2019. For *A. islandica*, seawater was maintained at a pH of 7.93 ± 0.09, temperature of 9 ± 1 °C, and salinity of 35 in the control conditions (Cameron 2020).

A detailed explanation of the collection and culturing of *C. virginica* is outlined in Downey-Wall et al. (2020). Adult *C. virginica* specimens were collected from three intertidal sites on Plum Island Sound, Massachusetts, USA (Site 1, 42°45’6” N, 70°50’13” W; Site 2,: 42°43’31” N, 70°51’18” W; 42°40’43” N, 70°48’49” W) in April 2017 and transferred to Northeastern University's Marine Science Center. The average *C.* virginica shell length was 9.23 ± 2.4 cm and shell width was 5.4 ± 0.8 cm (n=107). Specimens were acclimated to laboratory conditions for 33 days and then transferred to experimental tanks. Seawater salinity and temperature were monitored and maintained throughout the experiment. *C.*

virginica seawater was maintained at a temperature of 18.2 ± 1 °C, and salinity of 31 . *C. virginica* were exposed to control (mean pCO_2 ± SE = 570 ± 14 ppm; $\Omega_{calcite}$ = 2.95 ± 0.30), moderate OA (990 ± 29 ppm, $\Omega_{calcite}$ = 1.93 ± 0.32), or high OA (2912 ± 59 ppm, $\Omega_{calcite}$ = 0.75 ± 0.09) treatments. Target pCO_2 treatment was achieved by mixing compressed pCO_2 and compressed ambient air using solenoid-valve-controlled mass flow controllers at flow rates that target pCO_2 conditions. The treated seawater was introduced to the flow-through aquaria at a rate of 150 mL min^{-1}. For the acidification experiment, tank salinity, temperature, and DIC and TA were measured for the duration of the experiment and used to calculate pH (total scale), $\Omega_{calcite}$, $[CO_3^{2-}]$, $[HCO_3^-]$, $[CO_2]$, and pCO_2 of each tank using CO2SYS version 2.1 (Pierrot et al. 2011; Downey-Wall et al. 2020). Measured and calculated seawater parameters are reported in Table 1. Oysters were fed 1% Shellfish Diet 1800® twice daily following best practices outlined in Helm and Bourne (2004).

	Control *A. islandica*	Control *C. virginica*	Moderate OA *C. virginica*	High OA *C. virginica*
	Measured seawater parameters			
pH (total scale)	7.93 ± 0.09	8.01 ± 0.08	7.75 ± 0.07	7.29 ± 0.11
DIC (µmol/kg)	n/d	1966 ± 44	1998 ± 212	2177 ± 160
TA (µmol/kg)	n/d	2120 ± 46	2120 ± 42	1511 ± 40
Mg/Ca (mol/mol)	5.13 ± 0.07	5.15 ± 0.07	5.23 ± 0.06	5.12 ± 0.03
$\delta^{26}Mg$ (‰)	-0.82 0.06 ‰	-0.77 ± 0.01	-0.82 ±0.03	-0.76 ± 0.09
B/Ca (mol/mol)	41.75 ± 1.52	41.66 ± 1.07	43.08 ± 2.9	42.11 ± 1.8
$\delta^{11}B$ (‰)	39.88 ± 0.13	40.29 ± 0.33	39.39 ± 0.33	39.82 ± 0.33
	Calculated seawater parameters			
pCO_2 (ppm)	n/d	570 ± 90	990 ± 173	2912 ± 373
$[CO_3^{2-}]$ (µM)	n/d	120 ± 12	79 ± 13	31 ± 4
$\Omega_{Calcite}$	n/d	2.95 ± 0.30	1.93 ± 0.32	0.75 ± 0.09
$\Omega_{Aragonite}$	n/d	1.89 ± 0.19	1.24 ± 0.21	0.48 ± 0.06
$\delta^{11}B$-calculated pH (total scale)	7.76 ± 0.07	8.12 ± 0.09	8.06 ± 0.10	8.01 ± 0.08
$\triangle pH_{SW}$-$\delta^{11}B_{pH}$	0.17	0.64	0.77	0.88

Table 1. Seawater carbonate chemistry parameters (pH, DIC, TA, Ω, δ^{11}B-calculated EPF pH, and △pH) for both *C. virginica* and *A. islandica* under control conditions and *C. virginica* for OA conditions.. Seawater geochemical parameters (Mg/Ca, δ^{26}Mg, B/Ca, δ^{11}B) for both *C. virginica* and *A. islandica* under control conditions and *C. virginica* for OA conditions. Parameters that were unable to be not measured due to insufficient sample size or unable to be calculated are marked with 'n/d.'

2.2 Calcification rate measurements

Net calcification rate for *C. virginica* specimen (n=35) was calculated in Downey-Wall et al., (2020) using the buoyant weighing technique. Buoyant weight was measured by submerging oysters in a 27.65 liter tank (48 cm long, 24 cm wide and 24 cm deep) filled with seawater. Specimens were placed on a bottom-loading scale (Cole Parmer Symmetry S-PT 413E, precision= 0.001 g) and weighed three times. At the end of the experiment, an empirical linear relationship was created between buoyant weight and dry shell weight of shucked oysters following the same methodology in Ries et al. (2009). The residual mean squared error (RMSE) for the dry weight/buoyant weight model was 1.939 mg. Calcification was calculated as the difference in calculated dry weight at the start and end of the experiment over the number of days. This number was then divided by the initial weight and multiplied by 100 to get the percent change in calcification.

2.3 Extrapallial fluid sampling

Sampling of the extrapallial fluid (EPF) for both species was previously described in Downey-Wall et al. (2020). Briefly, a hole was drilled onto the shell to expose the EPF cavity, a port was inserted and sealed with epoxy to directly sample the EPF with a syringe and prevent seawater intrusion (Figure 1). Oysters recovered for 4 days before being transferred to experimental tanks for acclimation before the experiment. To sample the EPF, oysters were removed from the tanks and EPF was extracted by inserting a sterile 5 mL syringe with a flexible 18-gauge polypropylene tip through the port. EPF samples were stored in 2 mL microcentrifuge tubes and refrigerated at 6˚C for further analysis. EPF pH (Total scale) was measured directly after extraction using a micro-pH probe. EPF measurements were collected at the end of the experiment, on day 71, for *C. virginica* and day 14 for *A. islandica*. EPF pH diel variability was also explored by measuring EPF pH at 6 timepoints to produce time series for both species in a 24-hour period.

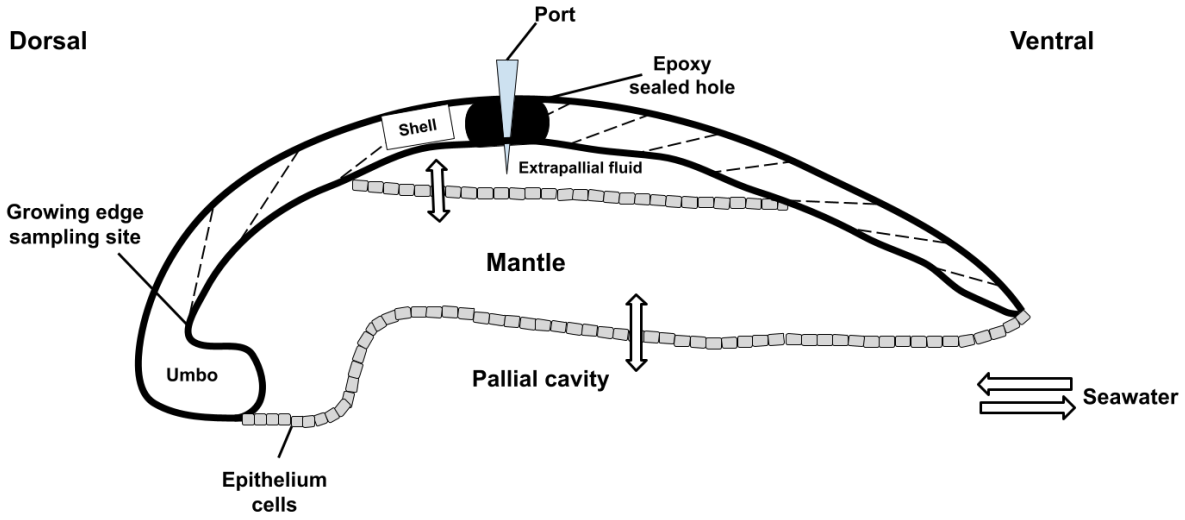

f 01

Figure 1. Schematic of a bivalve cross section from the dorsal to the ventral sides. Seawater enters the pallial cavity and ions can diffuse or be transported across the mantle organ to the extrapallial fluid space. A hole was drilled through the top of the shell into the extrapallial fluid space and sealed with epoxy following port insertion. Shell material was drilled on the inner side of the growing edge of the shell to sample new growth.

2.4 Shell sampling

Following EPF extraction, bivalves were shucked and cleaned in 90% ethanol. The cleaned shells were dried at room temperature for 48 hours and sealed in plastic bags for analysis. Shells were cut into cross sections from the hinge to the margin using a circular saw. Shells were rinsed with ethanol during sectioning to prevent mineralogical changes from heat exposure. For skeletal geochemical and elemental ratio analysis, the inner (lamellar) layer of the oyster shell was gently shaved with a diamond-tipped Dremel tool. Care was taken to ensure sampling the most recently deposited material right near the growing edge of the bivalve, located below the umbo of the oyster shell (Figure 1). Cross sections showed growth bands and aided in sampling the newest growth under experimental conditions. For *A. islandica*, we wanted to compare ambient conditions, so new growth was not necessary to sample. About 5 mg of ground powder was stored in sealed microcentrifuge tubes.

2.4 Elemental ratio analysis

For the shells, about 2.5 mg of powder was sub-sampled from each specimen shell and oxidatively cleaned with a 0.3 % hydrogen peroxide in 0.1 N sodium hydroxide solution to remove organic matter as described in Barker et al. (2003). Carbonate samples were dissolved in 1 N double-distilled HCl. Elemental ratios were measured on a Thermo Fisher Scientific Element XR HR-ICP-MS at the PSO (Plouzané, France) after Ca analyses on an Agilent ICP-AES Varian 710 at the University of California, Los Angeles (UCLA, Los Angeles, USA). Data quality and external reproducibility were maintained and quantified via repeated measurements of international standard JC_P-1 during a particular session (Gutjahr et al., 2021). Typical measured concentrations of procedural blanks for the trace element analyses for sessions in which samples are diluted to 30 ppm Ca are $^{7}Li < 3\%$, $^{11}B < 4\%$, $^{25}Mg < 0.1\%$, $^{87}Sr < 0.1\%$, and $^{43}Ca < 0.1\%$. Typical analytical uncertainties on the X/Ca elemental ratios are 0.3 µmol/mol for Li/Ca, 21 µmol/mol for B/Ca, 0.09 mmol/mol for Mg/Ca, and 0.01 mmol/mol for Sr/Ca (2 SD, n = 28).

For EPF and seawater samples, 10 µL of sample was added to 490 µL of a solution of 0.1 N HNO_3/0.3 M HF. Mono-elemental solution of indium was added to reach a concentration of 1 ppb to monitor any matrix effect or drift of the instrument during a particular session. Standards were prepared by diluting an in-house seawater standard spiked with indium. International standards NRC-NASS-6 was used to ensure quality of the data.

2.5 Boron isotope analyses

Boron purification for the different samples was achieved via microdistillation following the method described in Guillermic et al. (2021) and originally developed by Gaillardet et al. (2001) and modified for Ca-rich matrix by Wang et al. (2010). Approximately 2.5-3.0 mg of oxidatively cleaned shell powders were dissolved in 1N HCl. For the EPF, 25 µL of EPF was added to 40 µL of 1N HCl. For the seawater, 50 µL of concentrated HCl was added to 450 µL of seawater. 60µL of each of the solutions was loaded for microdistillation. Boron isotopes were analyzed at the Pôle Spectrométrie Océan (PSO), Plouzané, on a Thermo Neptune inductively coupled plasma mass spectrometry (MC-ICP-MS) equipped with 10^{11} Ohm Faraday cup.

The certified boron isotope liquid standard ERM© AE120 ($\delta^{11}B$ = -20.2 ± 0.6 ‰, Vogl et al.,, 2011) was used to monitor reproducibility and drift during each session. Samples measured for boron isotopes in carbonates were typically run at 80 ppb B (~30 ng B per <0.5 mL), whereas samples of EPF and seawater were typically run at 150-200 ppb B (~150 ng B per mL). Sensitivity on ^{11}B was 10 mV/ppb B (e.g., 10 mV for 1 ppb B) in wet plasma at 50 µL/min sample aspiration rate. Procedural boron blanks ranged from 0.3 to 0.4 ng B and the acid blank during analyses was measured at 3 mV on the ^{11}B, indicating a total blank contribution of <2% of the sample signal with no memory effect within and across sessions. External reproducibility was ensured by the measurements of carbonate standard microdistilled at the same time as the samples. Results for the isotopic composition of the JC_P-1 is $\delta^{11}B$ =24.67 ± 0.28 ‰ (2 SE, n=41), within error of published values (24.36 ± 0.45 ‰, 2SD, Gutjahr et al., 2021).

2.6 Magnesium isotope analyses

Carbonate samples were dissolved in 0.1 N buffered acetic acid ammonium hydroxide solution over four hours in a sonicator. Samples were then centrifuged and aliquots of the supernatant were transferred into cleaned 15 mL centrifuge tubes. Aliquots of the bulk supernatants were then diluted ~30-fold and calcium and magnesium were separated and purified in different runs via a Thermo-Dionex ICS-5000+ ion chromatograph equipped with a fraction collector according to established methods outlined by Husson et al. (2015). EPF samples contained organics that obscured elution profiles, thus limiting the elemental yield and purification. Therefore, samples were digested on a hot plate in hydrogen peroxide and nitric acid to remove organics prior purification. Seawater and EPF samples were purified through the Thermo-Dionex ICS-5000+ ion chromatograph using another elution method than for carbonate samples. Seawater and carbonate standards were also purified at the same time to ensure quality of the method.

Samples were then dried and then rehydrated in a solution of 2% nitric acid. Magnesium isotopic ratios were measured at Princeton University using a Thermo Neptune+ (MC-ICP-MS) spectrometer according to methods outlined in Higgins et al. (2018) and Ahm et al. (2021). Samples were introduced via an ESI Apex-IR sample introduction system. Magnesium isotope ratios ($^{26}Mg/^{24}Mg$) were measured in low resolution mode, with every sample bracketed by the analysis of standards. Results are reported relative to the Dead Sea Magnesium-3 standard (DSM-3). Long term external precision on magnesium isotope results at the Higgins Lab (Princeton) was determined through repeated measurements of the Cambridge-1 standard (-2.59 $\pm$ 0.07‰, 2 SD, n = 19) and modern seawater (-0.82 $\pm$ 0.14 ‰, 2 SD, n = 21) and is reported in Ahm et al. (2021). Measured standards during the analytical session are given for the Cambridge-1 standard (-2.60 $\pm$ 0.20 ‰, 2 SD, n = 2) and for modern seawater (-0.82 $\pm$ 0.06 ‰, 2 SD, n=2).

2.7 Calculation of boron proxies and EPF carbonate chemistry

The use of boron proxies to reconstruct pH and [CO_3^{2-}] of the precipitating solution (i.e., the organism's calcifying fluid) is based upon boron speciation and fractionation in seawater (Hemming and Hanson, 1992; Hönisch et al., 2004). In seawater-type solutions, the speciation of boric acid [$B(OH)_3$] and borate ion [$B(OH)_4^-$] varies as a function of pH (Hemming and Hanson 1992). In addition to the pH dependence of their relative abundances, the boron proxy also relies upon the large isotopic fractionation between the two boron species (Klochko et al., 2006, Nir et al., 2015). A key assumption of the proxy is that boron, in the form of borate ion, is the predominant form incorporated into the crystal lattice of calcite via carbonate ion substitution during the precipitation of calcium carbonate (Hemming and Hanson 1992). The $\delta^{11}B$ of the carbonate ($\delta^{11}B_{CaCO3}$) should then, in theory, reflect the boron isotopic composition of the borate ion ($\delta^{11}B_{B(OH)4-}$) in the bivalve calcifying fluid (extrapallial fluid), which in turn reflects pH of the calcifying (extrapallial) fluid.

The boron isotopic signature of the shell ($\delta^{11}B_{carb}$) was used to calculate pH of the calcifying fluid (pH_{CF}) using the following equation (Hemming and Hanson, 1992; Zeebe and Wolf-Gladrow, 2001):

$$pH_{cf} = pK_B - \log\left(\frac{\delta^{11}B_{SW} - \delta^{11}B_{carb}}{\delta^{11}B_{SW} - \alpha * \delta^{11}B_{carb} - \varepsilon}\right) \quad \text{eq. 1}$$

In equation 1, pK_B is the dissociation constant, $\delta^{11}B_{sw}$ represents the measured boron isotopic composition of seawater, $\delta^{11}B_{carb}$ represents the boron isotopic composition of the shell, and α/ε represents the boron isotopic fractionation factor/ fractionation between boric acid and borate ion (Klochko et al. 2006).

The saturation state of calcite (Ω_{cacite}) and aragonite ($\Omega_{aragonite}$) of the EPF for each species were calculated using temperature, salinity, pressure, measured EPF Ca^{2+}, measured EPF Mg^{2+}, pH either from microelectrode pH or $\delta^{11}B$-calculated pH, and literature values of DIC (3000 for *A. islandica* from Stemmer et al. 2019, and 4200 for *C. virginica* from McNally et al., 2022). The saturation states were calculated using Seacarbx with maximum input of Mg^{2+} allowed by the code for samples presenting higher EPF Mg^{2+} than the limit allowed by the code (Raitzsch et al., 2021). Those saturation state values are limited by the fact that no direct measurements of EPF DIC was performed during this study, and a range of Ca^{2+} and Mg^{2+} values were measured in the EPF, resulting in a range of calculated saturation states. The apparent partition coefficient calculated as the ratio of E/Ca for the mineral over the E/Ca for seawater.

2.8 Statistical analysis

All statistical tests were performed and data graphed using GraphPad Prism software version 9 (GraphPad Software Inc.; San Diego, CA, USA). Prior to statistical analyses, a Shaprio-Wilks test was run to determine normality and a Brown-Forsythe test was used to determine heterogeneity of variance of residuals. Only two comparative t-test data did not meet requirements, so a nonparametric Mann-Whitney u test was run in place of a t-test. T-test and Mann-Whitney u tests were performed in order to test whether there was a difference between seawater and EPF geochemical parameters and between the EPF of both species under ambient conditions. A one-way ANOVA with pH as a three level factor was used to test whether pH had a significant effect on our geochemical data. ANOVA and t-test significance was achieved if the p-value was less than 0.05. Regression analysis was performed on GraphPad Prism and significance was denoted if the slope of the regression was statistically non-zero.

3 Results

3.1 Culturing experiment, calcification rates, seawater and EPF chemistry

C. virginica specimens were previously cultured in experimental tanks with seawater that was continuously bubbled with gas mixtures comprising three pCO_2 levels: 400 ppm, 900 ppm, 2800 ppm (Downey-Wall *et al.*, 2020). The tank seawater saturation states of calcite ($\Omega_{calcite}$) was calculated for *C. virginica* under the ocean acidification experiment and not *A. islandica*. As seawater pCO_2 increased, seawater $\Omega_{calcite}$ decreased. Only the highest pCO_2 treatment produced calcite

saturation states $\Omega_{calcite} < 1$, which does not favor calcification (Table 1). Similarly to $\Omega_{calcite}$, calcification rates were also only measured for the *C. virginica* OA experiment. pCO_2 treatment had a significant effect on *C. virginica* calcification, with the percent change in calcification per day decreasing with increasing pCO_2. There was also variability in calcification between specimens within each treatment (Fig 2a).

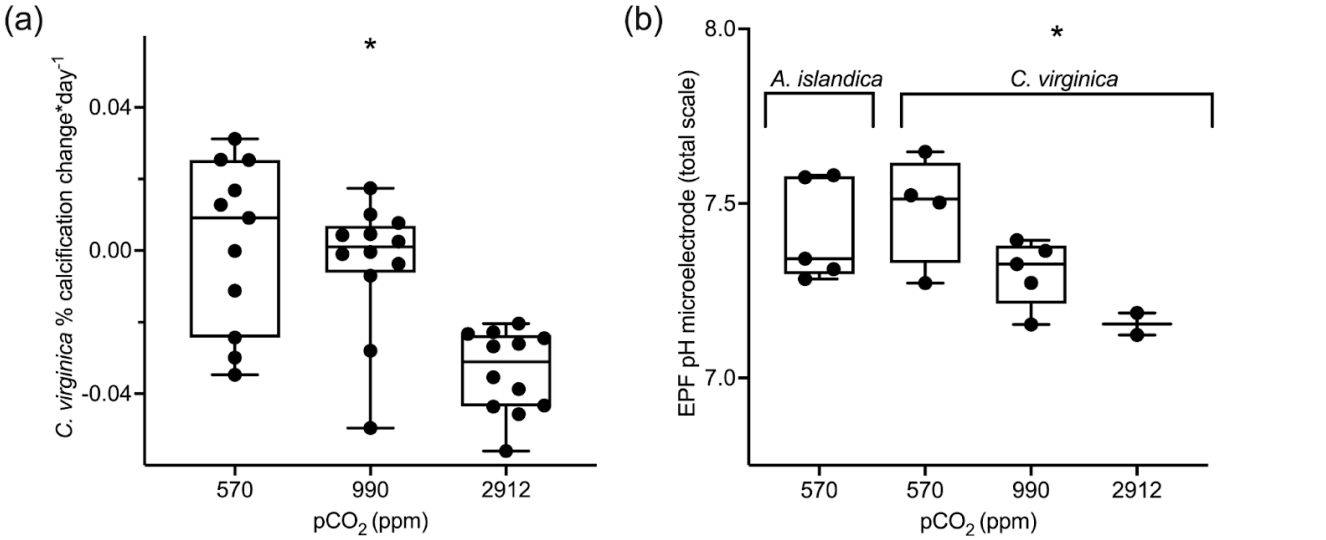

f02

Figure 2. (a) Box plots showing percent calcification change over the experiment for *C. virginica* for each treatment. (b) Averaged microelectrode EPF pH for *A. islandica* under control conditions and *C. virginica* for OA treatments. Stars denote a statistically significant ANOVA (at significance $p < 0.05$).

In this study, we present unpublished EPF pH microelectrode data for *A, islandica* cultured at a single control condition (400 ppm pCO_2) and we present published EPF microelectrode data for the *C. virginica* acidification experiment of Downey-Wall et al. (2020). At control seawater conditions the EPF pH of *A. islandica* was 7.41, compared to 7.48 for *C. virginica.* The EPF pH of both species were not statistically different (t-test $p>0.05$) and the average EPF pH of both species was well under seawater pH (Fig 2b). Additionally pCO_2 treatment also had a significant effect on *C. virginica* EPF pH (ANOVA p-value<0.05), with microelectrode measure EPF pH decreasing as pCO_2 increased (Fig 2b). Downey-Wall et al. (2020) also report that pCO_2 treatment had a significant effect on EPF pH (linear model, $p<0.05$) and that at the highest pCO_2 treatment, EPF pH was significantly lower than seawater pH (post hoc p-value<0.05 see Downey-Wall *et al*., 2020). We report the change in pH (ΔpH) for both species as the (seawater pH - EPF pH). The ΔpH for *A. islandica* was 0.52 and was similar to the control condition ΔpH for *C. virginica* which was 0.53 (Table 2). Under OA treatments, ΔpH for *C. virginica*

decreased with decreasing seawater pH. The ΔpH for the control treatment was 0.53, the moderate OA treatment was 0.46, and the high OA treatment was 0.08.

	Control *A. islandica*	Control *C. virginica*	Moderate OA *C. virginica*	High OA *C. virginica*
	EPF geochemistry			
EPF pH	7.41 ± 0.14	7.48 ± 0.15	7.29 ± 0.10	7.21 ± 0.10
$\triangle pH_{SW-EPF}$	0.52	0.53	0.46	0.08
Mg/Ca	4.25 ± 0.67	4.55 ± 0.50	5.73 ± 0.34	5.58 ± 0.46
$\delta^{26}Mg$	-0.69 ± 0.1	-0.88 ± 0.06	-0.87 ± 0.07	-0.9 ± 0.1
B/Ca	31.17 ± 4.87	33.66 ± 2.81	42.22 ± 3.33	43.26 ± 2.82
$\delta^{11}B$	39.5 ± 0.4	39.3 ± 1.0	38.9 ± 0.4	n/d
	Shell geochemistry			
Mg/Ca	0.8 ± 0.2	13.8 ± 1.7	13.4 ± 2.3	12.3 ± 1.5
$\delta^{26}Mg$	n/d	-3.2 ± 0.1	-3.1 ± 0.1	-3.0 ± 0.2
B/Ca	57 ± 17	114 ± 22	125 ± 11	124 ± 9
$\delta^{11}B$	15.2 ± 0.4	18.3 ± 0.5	16.9 ± 0.5	16.8 ± 0.3

Table 2. Measured extrapallial fluid (EPF) carbonate chemistry parameters (pH, DIC, TA, Ω, $\delta^{11}B$-calculated EPF pH, and △pH) for both *C. virginica* and *A. islandica* under control conditions and *C. virginica* for OA conditions. Extrapallial fluid and shell geochemical parameters (Mg/Ca, $\delta^{26}Mg$, B/Ca, $\delta^{11}B$) for both *C. virginica* and *A. islandica* under control conditions and *C. virginica* for OA conditions. Parameters that were unable to be not measured due to insufficient sample size or unable to be calculated are marked with 'n/d.'

3.2 Comparison of *A. islandica* and *C. virginica* geochemistry of seawater, EPF, and bivalve shell

There was a significant decrease in EPF Mg/Ca compared to seawater Mg/Ca for both *A. islandica* and *C. virginica* (t-test, n=2, p-value<0.05; Fig 3a-b). The Mg/Ca of *C. virginica* EPF was 4.55± 0.50 mol/mol and significantly higher than

303 *A. islandica* EPF which was 4.25±0.67 mol/mol (Fig 3d; Table 2). For both species, the low EPF Mg/Ca versus seawater
304 Mg/Ca was driven by higher Ca^{2+} concentrations in the EPF relative to seawater (Fig 3h-i). Considering the elemental
305 concentrations alone, instead of as a ratio, there was no significant difference in EPF Mg^{2+} or Ca^{2+} concentrations between
306 species (Fig 3g and 3j). Shell Mg/Ca for the calcitic *C. virginica* was 13.8±1.7 mmol/mol and significantly higher than the
307 aragonitic *A. islandica* shell which was 0.8±0.02 mmol/mol, in line with shell polymorph mineralogy. The apparent partition
308 coefficient (K_{Mg}) between the seawater and the shell was 0.003 in *C. virginica* and 0.002 in *A. islandica* (Table 3). K_{Mg}
309 between EPF and shell was 0.003 in *C. virginica* and 0.002 in *A. islandica*. K_{Mg} between seawater and the EPF is 0.9 for *C.*
310 *virginica* and 0.8 for *A. islandica* (Table 3). *C. virginica* seawater and EPF $\delta^{26}Mg$ were -0.77 ± 0.01 ‰ and -0.88 ± 0.06 ‰,
311 respectively and displayed a significant decrease in EPF $\delta^{26}Mg$ compared to seawater for *C. virginica* (t-test, n1=3 n2=5,
312 p-value< 0.05; Fig 3k-l). For *A. islandica*, seawater and EPF $\delta^{26}Mg$ were -0.82 ± 0.06 ‰ and -0.69 ± 0.01 ‰, respectively,
313 but no statistical analysis could be done between the two reservoirs owing to the small sample size (Table 1 and 2). The
314 average shell $\delta^{26}Mg$ for *C. virginica* was -3.2 ± 0.1‰, but *A. islandica* shell $\delta^{26}Mg$ could not be analyzed because of low
315 shell [Mg^{2+}] content and limited sample material.

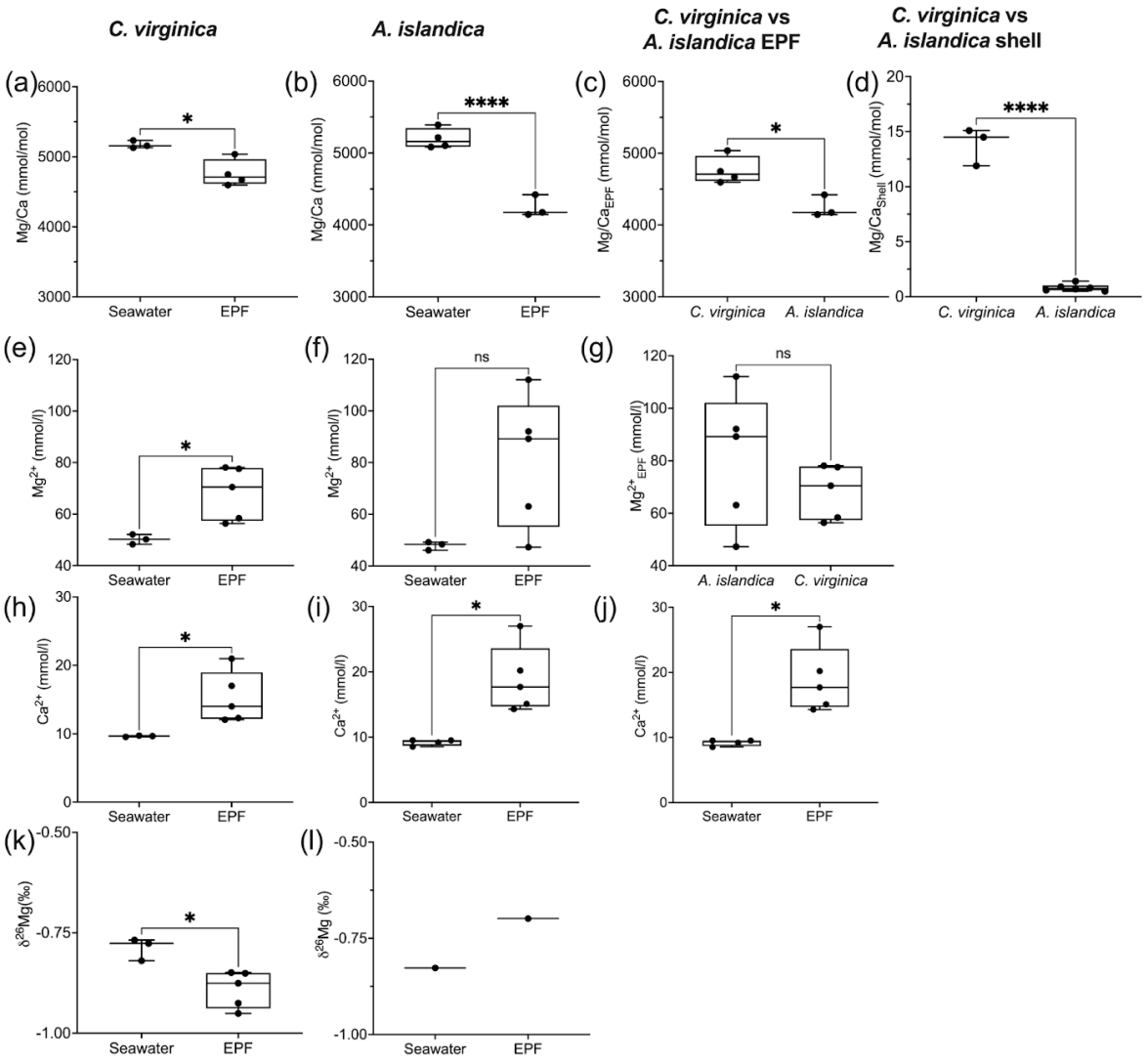

f 03

316

317 **Figure 3.** Box plots of Mg/Ca comparing seawater and extrapallial fluid for (a) *C. virginica* and (b) *A. islandica*, (c)
318 comparing EPF Mg/Ca between species, and (d) shell Mg/Ca between species. Box plots of [Mg^{2+}] comparing seawater and
319 extrapallial fluid for (e) *C. virginica* and (f) *A. islandica*, (g) comparing EPF [Mg^{2+}] between species. Box plots of [Ca]
320 comparing seawater and extrapallial fluid for (h) *C. virginica* and (i) *A. islandica*, (j) comparing EPF [Ca] between species.
321 Box plots of δ^{26}Mg comparing seawater and extrapallial fluid for (k) *C. virginica* and (l) *A. islandica*. Stars denote
322 statistically different means and 'ns' signify non significant mean differences in a pairwise t-test or Mann-Whitney u test (at
323 significance $p < 0.05$). No comparison was tested on (l) due to limited sample size.

324

325

	A. islandica		*C. virginica*		
		pCO_2	400	900	28000
K_{Mg}	0.0002		0.003	0.002	0.002
K_B	0.001		0.003	0.003	0.003

Table 3. Partition coefficients between seawater and the mineral for Mg/Ca and B/Ca.

A. islandica EPF B/Ca was 27.91 ± 4.87 mmol/mol and was significantly lower than seawater B/Ca which was 41.75 ± 1.52 mmol/mol (t-test, n1=7 n2=5, p-value<0.05, Fig 4a). *C. virginica* EPF B/Ca was 41.66 ± 1.07 mmol/mol and was significantly lower than seawater B/Ca which was 33.66 ± 2.81 mmol/mol (t-test, n1=6 n2=5, p-value<0.05 Fig 4b) The boron concentration was not significantly different between seawater and EPF for both *C. virginica* and *A. islandica* (Fig 4e-f). There was no significant difference in shell or EPF B/Ca between *C. virginica* and *A. islandica* (Fig 4c-d). The apparent partition coefficient (K_B) between the seawater and the shell was 0.003 in *C. virginica* and 0.001 in *A. islandica*. K_B between EPF and shell was 0.003 in *C. virginica* and 0.002 in *A. islandica*. K_B between seawater and the EPF is 0.8 in *C. virginica* and 0.7 for *A. islandica* (Table 3). There was no significant difference in $\delta^{11}B$ between seawater and EPF for both species in the control condition (Fig 4h-l). There was also no significant difference in EPF $\delta^{11}B$ between species(Fig 4j); however, there was a significant difference in shell $\delta^{11}B$ between *C. virginica* and *A. islandica* (t-test, n1=10 n2=3, p-value<0.05, Fig 4k). Under control conditions, shell $\delta^{11}B$ was measured to be 15.26 ± 0.41‰ (2 SD, n=3) for *C. virginica* and 18.34 ± 0.59 ‰ (2 SD, n = 3) for *A. islandica*.

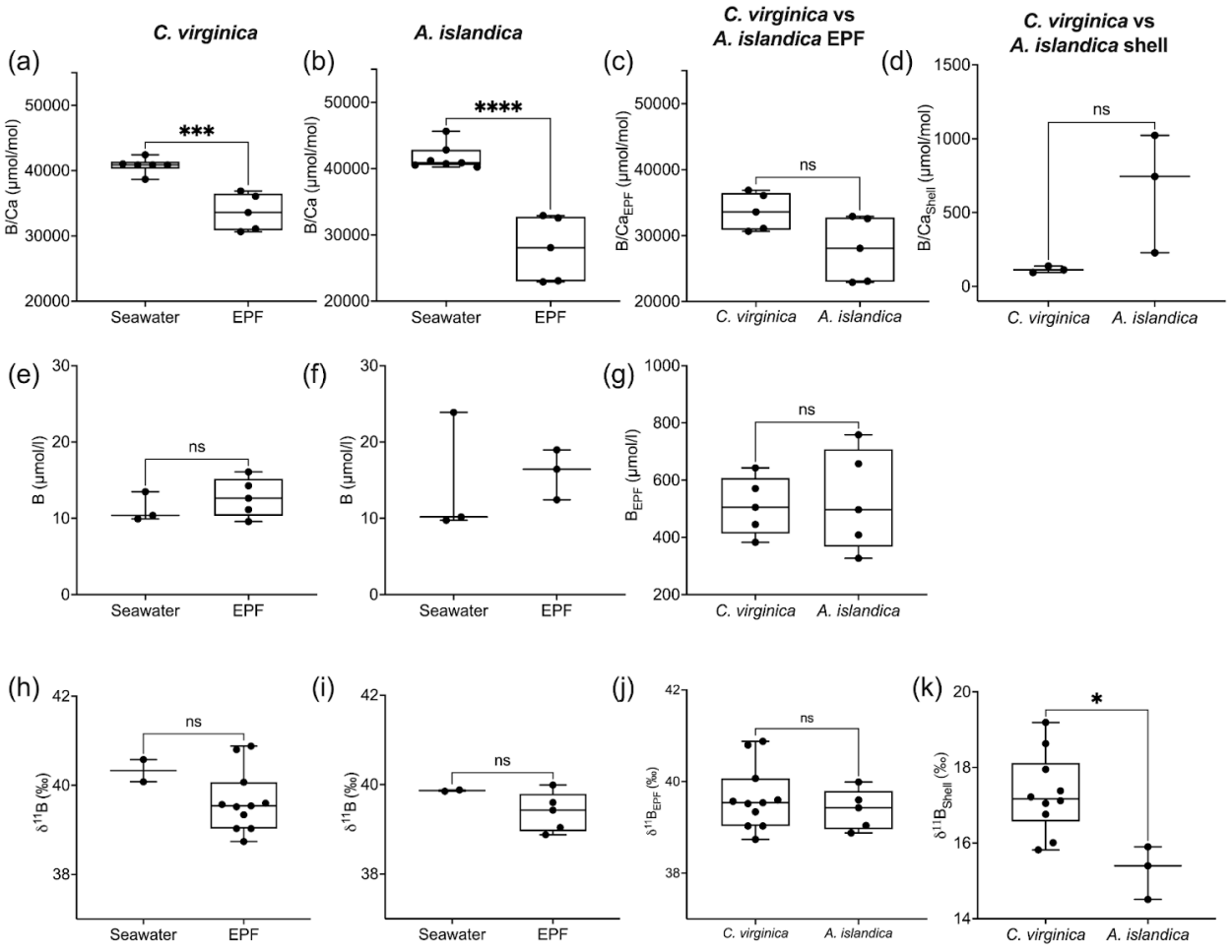

f 04

Figure 4. Box plots of B/Ca comparing seawater and extrapallial fluid for (a) *C. virginica* and (b) *A. islandica*, (c) comparing EPF B/Ca between species, and (d) shell B/Ca between species. Box plots of [B] comparing seawater and extrapallial fluid for (e) *C. virginica* and (f) *A. islandica*, (g) comparing EPF [B] between species. Box plots of $\delta^{11}B$ comparing seawater and extrapallial fluid for (h) *C. virginica* and (i) *A. islandica*, comparing EPF $\delta^{11}B$ between species, and (d) shell $\delta^{11}B$ between species. Stars denote statistically different means and 'ns' signify non significant mean differences in a pairwise t-test or Mann-Whitney u test (at significance $p < 0.05$).

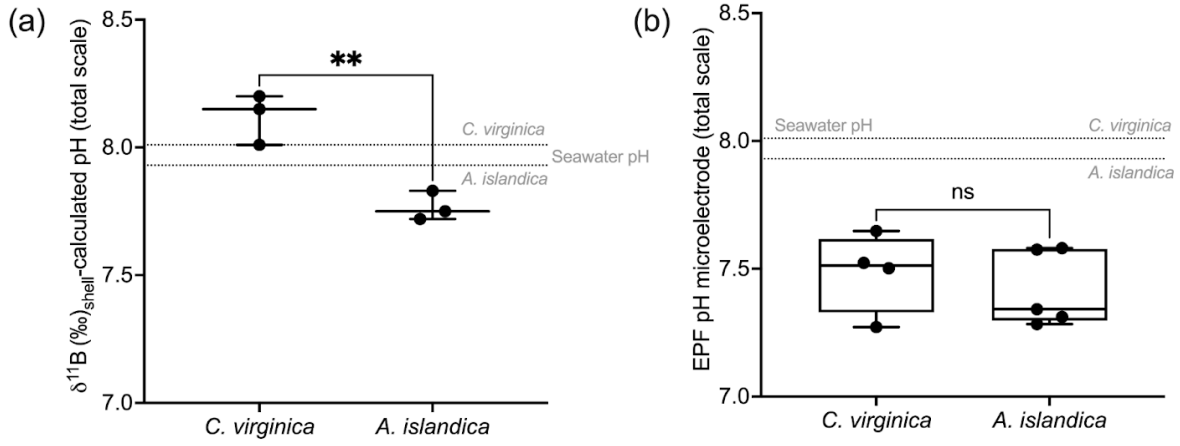

f 05

348

349

350 **Figure 5.** (a) Box plot of δ^{11}B-calculated pH for *C. virginica* and *A. islandica*. (b) Box plot of measured microelectrode pH
351 for *C. virginica* and *A. islandica*. The grey line shows seawater pH for *C. virginica* and *A. islandica*. Stars denote statistically
352 different means and 'ns' signify non significant mean differences in a pairwise t-test (at significance $p < 0.05$).

353 The control condition δ^{11}B-calculated EPF pH for *C. virginica* was 8.12 ± 0.08 ‰ (2 SD, n=3) and for *A. islandica*
354 was 7.93 ± 0.09 ‰ (2 SD, n=3), which yielded a statistically significant difference between the two species (t-test, n1=3
355 n2=3, p-value<0.05, Fig 5a). For *C. virginica*, the δ^{11}B-calculated EPF was 0.1 pH units higher than the seawater pH and 0.6
356 lower than measured EPF pH. Conversely, the *A. islandica* δ^{11}B-calculated EPF was 0.1 pH units lower than the seawater pH
357 and 0.3 higher than the measured EPF pH (Fig 59).

358

	Control *A. islandica* (Ωaragonite)	Control *C. virginica* (Ωcalcite)	Moderate OA *C. virginica* (Ωcalcite)	High OA *C. virginica* (Ωcalcite)
Ω using EPF pH (range)	1.7 (1.0-3.8)	3.7 (1.3-11.4)	1.1 (0.5-2)	0.9 (0.5-1.2)
Ω using δ^{11}B-calculated pH (range)	3.8 (2.9-6.7)	15.4 (6.7-37)	6.1 (3-11.7)	6.5 (3.4-9.7)

359

Table 4. Table of calculated saturation state (Ω) with respect to calcite (*C. virginica*) or aragonite (*A. islandica)* for the average EPF pH value based on microelectrode measurements or δ^{11}B-calculated EPF pH.

In Table 4, the EPF aragonite saturation state ($\Omega_{aragonite}$) for *A. islandica* and EPF calcite saturation state ($\Omega_{calcite}$) for *C. virginica* were calculated using the averaged measured EPF pH and averaged δ^{11}B-calculated EPF pH, averaged measured Mg^{2+} and Ca^{2+}, and literature values of DIC (3000 µmol/L for *A. islandica* taken from Stemmer et al. (2019) and 4200 µmol/L for *C. virginica* from McNally et al. (2022). Under control conditions, the *A. islandica* $\Omega_{aragonite}$ and *C. virginica* $\Omega_{calcite}$ that was calculated using δ^{11}B-calculated EPF pH and measured EPF pH (Table 4). Under the ocean acidification experiment, EPF $\Omega_{calcite}$ decreased with decreasing seawater pH when using either EPF pH or δ^{11}B-calculated EPF pH to calculate EPF $\Omega_{calcite}$. There were large differences in *A. islandica* $\Omega_{aragonite}$ and *C. virginica* $\Omega_{calcite}$ when using either EPF pH ($\Omega_{aragonite}$=1.7 and $\Omega_{calcite}$=3.7) or the δ^{11}B-calculated pH ($\Omega_{aragonite}$=3.8 and $\Omega_{calcite}$=15.4).

3.3 *C. virginica* ocean acidification experiment geochemistry

In the *C. virginica* acidification experiment, EPF but not shell Mg/Ca was found to increase as EPF pH decreased (regression, n=10, p-value<0.05; Fig 6a-b). OA treatment had a significant effect on shell Mg/Ca (ANOVA, n=10, p-value<0.05, Fig 6a-b). The concentration of both Ca^{2+} and Mg^{2+} in the EPF decreased with decreasing EPF pH (regression, n=10, p-value< 0.05; Fig 6c-d). However, when binning by seawater pH treatments, only the Ca^{2+} and Mg^{2+} of the ambient condition was significantly elevated compared to the moderate and high ocean acidification treatments (Tukey HSD, n1=4 n2=3, p<0.05, Fig 6c-d). The EPF and shell δ^{26}Mg did not change as a function of EPF or seawater pH (Fig 6e-f and 5e-f).

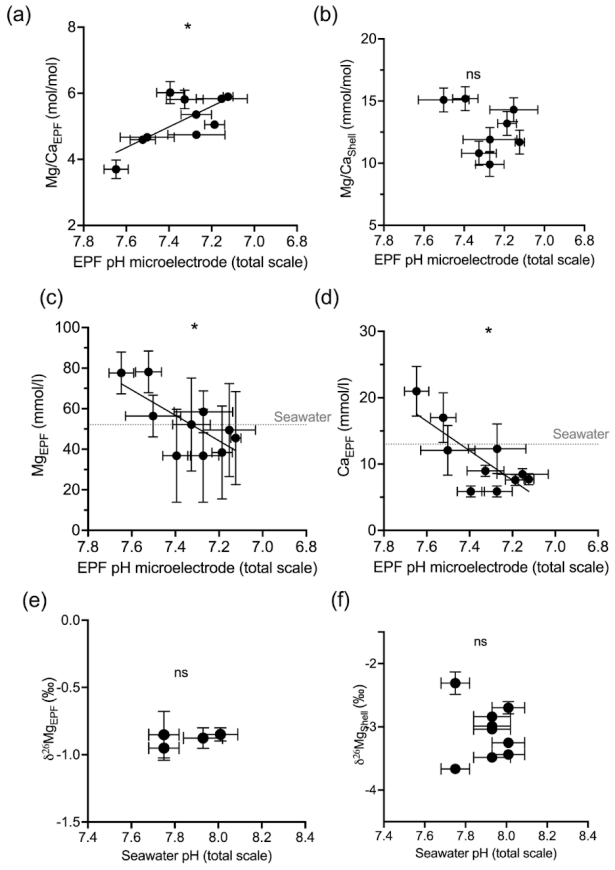

f 06

Figure 6. Scatter plots showing *C. virginica* individual specimen (a) EPF Mg/Ca and (b) shell Mg/Ca across corresponding microelectrode pH. Additionally, scatter plots (c) EPF Mg^{2+}, (d) EPF Ca^{2+}, (e) EPF $\delta^{26}Mg$, and (f) shell $\delta^{26}Mg$ across microelectrode EPF pH. Dotted gray lines on (c) and (d) show the average Mg^{2+} and Ca^{2+} seawater concentration, respectively. Stars denote statistically significantly nonzero regression slopes and 'ns' signify non significant regressions (at significance $p < 0.05$).

Under OA conditions, EPF B/Ca but not shell B/Ca was found to increase as seawater pH decreased (ANOVA p-value<0.05, compare Fig 7a-b). The EPF but not shell B/Ca was found to increase as EPF pH decreased (regression p-value< 0.05, Fig 7a-b). The boron concentration of the EPF, but not the shell, significantly decreased with decreasing EPF pH (regression p-value< 0.05, Fig 7c). The EPF B concentration increased with increasing seawater pH (ANOVA p-value<

0.05, Fig 7c); however, shell boron concentrations did not significantly change with seawater pH. Due to small EPF sample volume, EPF for the oysters in the lowest seawater pH treatment was not measured for $\delta^{11}B$. There was a significant difference in mean EPF $\delta^{11}B$ between the control pH treatment which was 39.39 ‰ and moderate pH treatment which was 38.92 ‰ (t-test, n1=11 n2=7, p-value<0.05, Fig 7e-f). The difference between seawater $\delta^{11}B$ and EPF $\delta^{11}B$ was 0.91 ‰ for the control treatment and decreased to 0.47 ‰ for the moderate pH treatment. Shell $\delta^{11}B$, but not EPF $\delta^{11}B$, significantly decreased with decreasing EPF pH (regression p-value<0.05, Fig 7e-f).

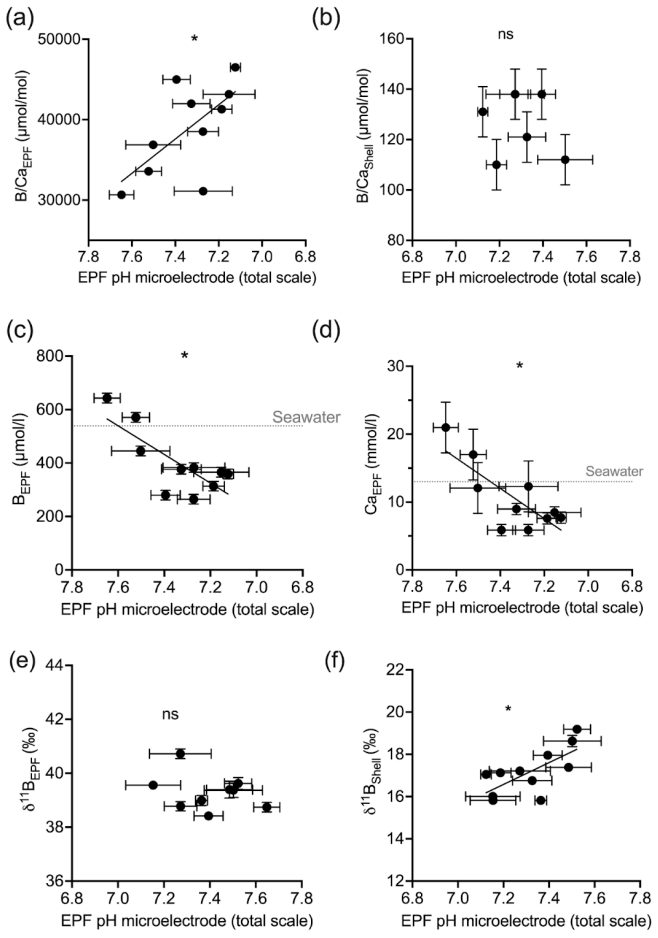

f 07

Figure 7. Scatter plots showing *C. virginica* individual specimen (a) EPF B/Ca and (b) shell B/Ca across corresponding microelectrode EPF pH. Additionally, scatter plots of (c) EPF B, (d) EPF Ca^{2+}, (e) EPF $\delta^{11}B$, and (f) shell $\delta^{11}B$ across microelectrode EPF pH. Dotted gray lines on (c) and (d) show the average B and Ca^{2+} seawater concentration, respectively. Stars denote statistically significantly nonzero regression slopes and 'ns' signify non significant regressions (at significance $p < 0.05$).

Fig 8a shows the measured EPF pH, the δ^{11}B-calculated EPF, and seawater to EPF 1:1 pH line graphed across the *C. virginica* acidification experiment. The slope of the measured microelectrode EPF pH versus seawater pH linear regression was 0.36, and lies below the seawater to EPF 1:1 pH line, but intersects the seawater to EPF 1:1 pH line at lowest pH/highest pCO_2 culture conditions (Fig 8). Conversely, the slope of the δ^{11}B-calculated EPF pH versus seawater pH linear regression was 0.14, lies above the seawater to EPF 1:1 pH line, but intersected the seawater to EPF 1:1 pH line at higher culture pH conditions (Fig 8).

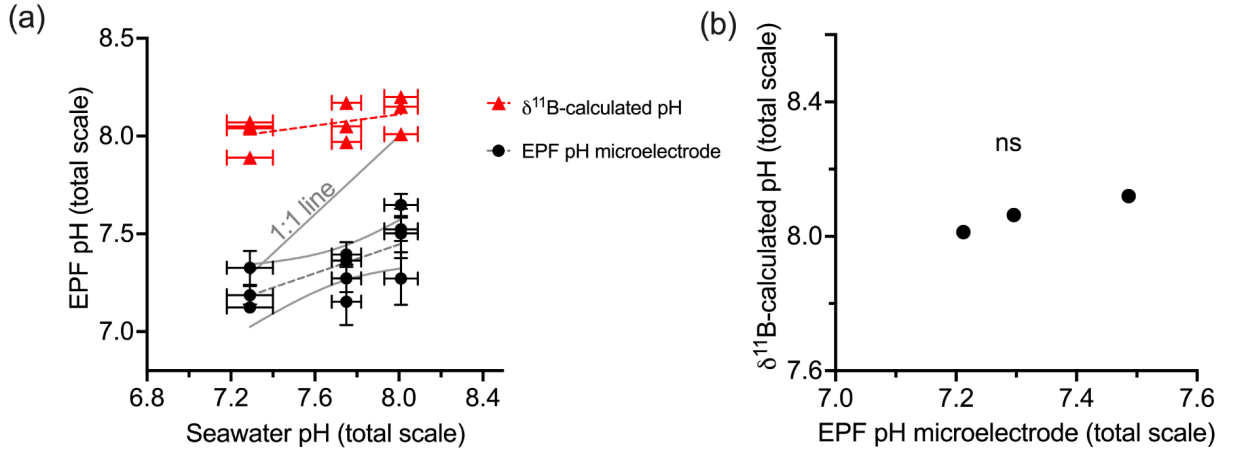

f 08

Figure 8. (a) Scatter plot of δ^{11}B-calculated pH and microelectrode EPF pH across seawater pH treatments. The gray line shows the 1:1 seawater to EPF pH line. The δ^{11}B-calculated pH regression line had a slope of 0.14. The microelectrode EPF pH line had a slope of 0.36. (b) shows the averaged δ^{11}B-calculated pH versus microelectrode EPF pH. The 'ns' signifies a non significant regression (at significance $p < 0.05$).

For the *C. virginica* acidification experiment, Downey-Wall et al., (2020) measured the EPF pH of individual specimens in each acidification treatment over a 24-hour period (n_{total}=108 and n=6 per time point per treatment). Fig 9 shows how the EPF pH for each individual fluctuated over 24 hours. Ambient treatment EPF pH ranged from 6.63-7.94, moderate OA treatment ranged from 6.68-7.88, and high OA treatment ranged from 6.78-7.47. The control treatment EPF pH of individuals did intersect the averaged seawater pH for the treatment tanks, however, the EPF pH in the moderate and high pH treatments fell below the corresponding average treatment seawater pH lines. For all treatments, the time series EPF pH lines fell below the corresponding treatment averaged δ^{11}B-calculated EPF pH line.

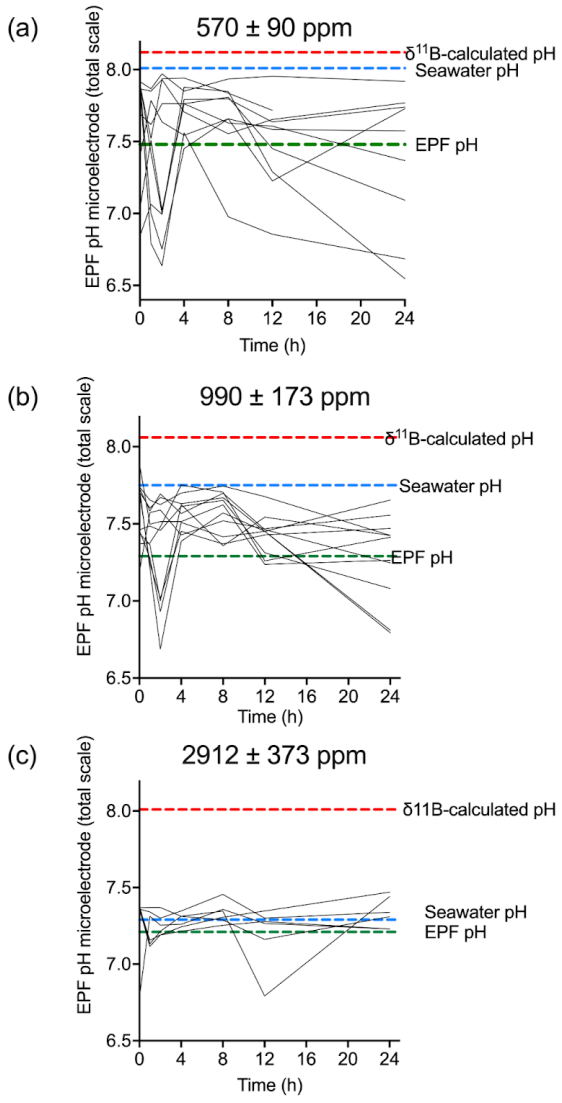

f 09

Figure 9. Time series (in hours) of microelectrode EPF pH over a 24 hour period for (a) control (n=10) (b) moderate (n=11) and (c) high pCO_2 treatments (n=6). Each line represents the microelectrode EPF pH for each individual specimen measured in that treatment. The red dotted line shows the corresponding average δ^{11}B-calculated pH for the treatment, the blue dotted line shows the average seawater pH for the treatment, and the green dotted line shows average EPF pH.

4. Discussion

4.1 Comparison of *A. islandica* and *C. virginica* Mg^{2+} and Ca^{2+} geochemistry of seawater, EPF, and bivalve shell

This study examined tripartite element and isotope fractionation between different reservoirs involved in the biomineralization of two bivalves species, aragonitic *A. islandica* and calcitic *C. virginica*. Marine bivalves source ions for internal fluids from seawater and previous studies by Crenshaw (1972) have highlighted that the extrapallial fluid is chemically different from seawater. The ions sourced from seawater are modulated either passively or actively across the outer mantle epithelium (OME) cells into the extrapallial cavity, where biomineralization occurs (Zhao et al., 2018). The exact mechanisms behind bivalve biomineralization is still a topic of active research and evidence has been put forth for several distinct pathways, primarily regulation of calcification constituents across the OME or transport of a precursor phase of $CaCO_3$ to promote calcification (Addadi et al., 2003; Checa 2018).

In this study we found that the extrapallial fluid is chemically distinct from seawater. Here we show that, under ambient conditions, both the EPF Mg/Ca and B/Ca of both *C. virginica* and *A. islandica* were lower than that of seawater, indicating that the EPF has a distinct geochemical make up from seawater (Fig 3). This is consistent with the anatomical understanding in bivalves that the extrapallial fluid is semi-isolated from seawater and its geochemistry can be influenced by ion fluxes across the OME as well as other ion pathways (Crenshaw 1972; Sillanpaa et al., 2018; Stemmer et al., 2019). However, we also find that for both Mg/Ca and B/Ca, this result is driven by an increase in absolute Ca^{2+} in EPF, so we do not find evidence for dilution or concentration of the absolute Mg^{2+} or B in the EPF (Fig 3). Previous work on bivalves has shown that magnesium can inhibit calcite crystal nucleation and there is evidence for exclusion of Mg^{2+} from the EPF (Lorens and Bender, 1977). In line with other studies, we show that *C. virginica* and *A. islandica* have lower Mg/Ca in EPF than seawater (Lorens and Bender, 1977; Planchon et al., 2013); however, we note that the EPF Mg/Ca trend is driven by changes in EPF Ca^{2+}. *C. virginica* and *A. islandica* EPF Mg/Ca were significantly different, with lower EPF Mg/Ca for *A. islandica*, possibly due to different controls over EPF Ca^{2+} between both species. The partition coefficient between EPF and the shell was calculated to be 0.003 for *C. virginica* 0.0002 for *A. islandica*, which is consistent with previous studies on bivalves and with the Mg/Ca mineralogical difference between the calcite produced by *C. virginica* and the aragonite produced by *A. islandica* (Ulrich et al. 2021).

We found that the EPF $\delta^{26}Mg$ of *C. virginica* was depleted compared to seawater $\delta^{26}Mg$ (Fig 3). Our $\delta^{26}Mg$ values for the EPF and shell were in line with previous work on bivalves (Planchon et al., 2013). Planchon et al. (2013) found a -0.23 ± 0.25 ‰ (2 SD, n=5) difference between EPF and seawater in the aragonitic manila clam, *Ruditapes philippinarum*. Similarly, in the present study, a difference of -0.11 ± 0.06 ‰ was observed for the calcitic *C. virginica*, but no $\delta^{26}Mg$ data were collected for *A. islandica* due to sample limitation. Both Planchon et al. (2013) and the present study show depleted EPF $\delta^{26}Mg$ relative to seawater $\delta^{26}Mg$, indicating a potential biological modulation of EPF Mg^{2+} which has been previously attributed to heavier isotopes being incorporated into soft tissues or magnesium fixation within organic molecules (Planchon et al., 2013). However, it is important to note that the difference between EPF and seawater $\delta^{26}Mg$ is low and the $\delta^{26}Mg$

fractionation between the shell and seawater (2.43‰) was slightly larger than but still in line with inorganic calcite precipitation studies (Mavromatis et al., 2013; Saulnier et al., 2012).

4.2 Comparison of *A. islandica* and *C. virginica* EPF pH and boron geochemistry of seawater, EPF, and bivalve shell

The boron isotopes and B/Ca proxies have been used as paleo-pH and CO_3^{2-} proxies, recording changes in seawater carbonate chemistry in the shells of foraminifera (e.g. Hemming and Hanson 1992; Sanyal et al., 2001; Foster and Rae, 2016). In different taxa however, there is evidence that these proxies monitor changes in the carbonate chemistry of the internal calcifying fluid, which may be different from seawater geochemistry (e.g. Allison and Finch 2010; Cornwall et al., 2017; Sutton et al., 2018; Guillermic et al., 2021). In the present study, we constrained the B/Ca and $\delta^{11}B$ of the main reservoirs involved in the biomineralization (seawater, extrapallial fluid, and shell) of *C. virginica* and *A. islandica.*

We found an incongruence between seawater pH, measured EPF pH and $\delta^{11}B$-calculated pH. For both *C. virginica* and *A. islandica* microelectrode EPF pH was lower than seawater pH. These findings are similar to previous work on bivalves which also show that the EPF pH is lower than seawater pH (Crenshaw 1972; Heinemann et al., 2012; Stemmer et al., 2019; Cameron et al. 2019). Microelectrode EPF pH between species was found to not be significantly different, indicating a similar downregulation in pH compared to seawater. However, our $\delta^{11}B$-based EPF pH was different between species (Fig 5). Using boron isotope systematics, this translated to a $\delta^{11}B$-calculated EPF pH of 7.76 ± 0.07 for *A. islandica* and 8.12 ± 0.09 for *C. virginica*. Although boron isotopes have been shown to probe the internal calcification fluid of certain taxa, like corals (e.g. Allison and Finch 2010), our results show an incongruence between measured EPF pH and $\delta^{11}B$-calculated pH.

4.3 *C. virginica* ocean acidification effects on Mg^{2+} and Ca^{2+} geochemistry of seawater, EPF, and bivalve shell

In the complementary study by Downey-Wall et al. (2020), it was found that the *C. virginica* calcification rates decreased with seawater pH (Downey-Wall et al., 2020; Fig 2). The reduction of calcification under ocean acidification conditions is well documented in other seawater pH experiments on different bivalve species (e.g., Ries et al., 2009; Beniash et al., 2010; Waldbusser et al., 2011; Downey-Wall et al., 2020). This result is consequential as the shell is important in protecting the animal from predation, desiccation, and the effects of transient changes in seawater chemistry (Gosling et al., 2008). Under ocean acidification treatments, the average microelectrode EPF pH of *C. virginica* was lower than seawater pH. This is in line with other simulated ocean acidification studies that also found a decrease in EPF pH (Michaelidis et al., 2005; Thomsen et al., 2013; Zittier et al.; 2015, Cameron et al., 2019; Downey-Wall et al., 2020). However, the change in pH between EPF and seawater pH (△pH) decreased with decreasing pH, resulting in an EPF pH that was closer to seawater pH under acidified conditions (Fig 8a, Fig. 9c).

Only *C. virginica* was cultured under ocean acidification (OA) treatments representing control, moderate, and high OA treatments. As mentioned above, the control experiment showed elevation of EPF Ca^{2+} and EPF Mg^{2+} relative to seawater. However, as EPF pH decreased, the EPF Ca^{2+} and Mg^{2+} significantly decreased as well (Fig 6). Ion transporters such as voltage gated Ca^{2+}-channels tend to also affect chemically similar ions like Mg^{2+} and a reduction of such a transporter could possibly explain the similar trends in Ca^{2+} and Mg^{2+} concentrations under OA (Hess et al., 1986). Under OA

conditions, EPF Ca^{2+} decreased to concentrations that were similar to or below seawater Ca^{2+}, indicating a reduced ability of the organism to upregulate these ions under OA conditions. Previous studies have found a similar tight coupling between pH and Ca^{2+}. For example, Stemmer et al. (2019) found synchronous patterns between pH and Ca^{2+} dynamics in *A. islandica* that they explained to be the result of calcium-transporting ATPase, which exchanges protons and calcium ions across the mantle and has proven to be important for acid-base regulation and calcium transport in bivalves (Stemmer et al., 2019; Sillanpaa et al., 2018; Sillanpaa et al., 2020). Although calcium transporting ATPase could explain this increase in Ca^{2+} under ambient conditions, this transport mechanism may be reduced under acidified conditions, thereby impairing the bivalve's ability to regulate protons and calcium ions in the extrapallial fluid, rendering EPF Ca^{2+} and pH more similar to that of seawater.

Alternatively, the simultaneous reduction in Ca^{2+} and Mg^{2+} under OA conditions could point to an ion storage mechanism. The reduction of both calcium and magnesium within the EPF under moderate and high OA treatments could possibly be linked to changes of storage and budgets of ions under stressful conditions (Mount et al., 2004; Johnstone et al., 2015; Wang et al. 2017). Further, several studies have highlighted significant changes in bivalve Ca^{2+} ion transport and storage in different extracellular and subcellular compartments associated with shell damage and repair under acidified conditions (Sillanpaa et al., 2016; Mount et al., 2004; Fitzer et al., 2016). Lastly, the EPF Ca^{2+} could simply reflect the balance between calcification and dissolution of the shell, as exemplified in a study on *C. virginica* conducted by Ries et al. (2016) which found that under similarly low saturation states, localized shell calcification was maintained despite net dissolution of the shell. Regardless of the exact mechanism, the reduction in extrapallial fluid Ca^{2+} under ocean acidification is a significant result that could impact the ability of bivalves to calcify by decreasing the $CaCO_3$ saturation state of the EPF.

4.4 *C. virginica* ocean acidification effects on boron geochemistry

Similarly to ambient conditions, the calculated $\delta^{11}B$-based pH for *C. virginica* is systematically higher than microelectrode EPF pH (Fig 8). Both $\delta^{11}B$-based pH and measured EPF pH record a decrease in pH under acidified conditions (regression $p<0.05$ for microelectrode pH). However, the offset between microelectrode EPF pH and the $\delta^{11}B$-calculated pH was 0.3 pH units and increased to 0.6 and 0.8 pH units for the moderate and high OA treatments, respectively (Fig 8). This demonstrates that, under OA conditions, the incongruence between $\delta^{11}B$ based pH and measured EPF pH increases and potentially renders the seawater pH proxy impractical, even after species-specific empirical calibration. Under OA conditions, shell $\delta^{11}B$ was not correlated with changes in seawater pH, but was significantly correlated to microelectrode pH (Fig 7f). These data indicate that microelectrode EPF pH does not fully resolve $\delta^{11}B$ vital effects or discrepancies.

However it is important to note the differences in timescales associated with $\delta^{11}B$-calculated EPF pH and microelectrode pH. Our microelectrode pH measurements, although averaged across several time points, show snapshots in time and are variable due different behavioral scenarios such asn open (feeding, high pH) and closed (respiring into a closed system, low pH) cycles. Conversely, the $\delta^{11}B$ approach represents EPF pH integrated average EPF pH over the interval that the sampled shell was formed, which could range from days to weeks. Furthermore, the $\delta^{11}B$ method will only record EPF pH at the site of calcification when the shell is forming, which can skew the archiving of the $\delta^{11}B$ pH signal in the shell to

higher values because the crystal only forms when saturation states and calcification rates are higher. This potential bias is also consistent with our δ^{11}B-calculated EPF pH data being higher than the microelectrode pH data, and similar to trends seen in corals (Cameron et al, 2022).

A possible explanation for the incongruence between δ^{11}B-based pH and measured EPF pH arises from boron isotope systematics. The boron isotope proxy assumes that only the charged borate ion is incorporated as BO_4 into the mineral but has been shown that boric acid can also be incorporated as BO_3, and NMR studies have shown the presence of BO_3 in the shells of different marine organisms (Rollion Bard et al., 2011; Cusack et al., 2015). However, the presence of BO_3 does not obviously translate to a strong bias in the δ^{11}B signature of the mineral due to the potential re-coordination of BO_4 to BO_3 within the crystal lattice (Klochko et al., 2009). A simple calculation shows that 14-17% boric acid incorporation could explain the observed difference between EPF pH and δ^{11}B-calculated pH for *C. virginica*, which could very well explain the discrepancy. Alternatively, shell δ^{11}B could also be affected by seawater or extrapallial fluid DIC, which bivalves are known to modulate under ambient and OA conditions (Crenshaw 1972, Stemmer et al., 2019). Gagnon et al. (2021) found that the shell δ^{11}B of deep-water coral is independently sensitive to changes in seawater DIC as a result of diffusion of boric acid (Gagnon et al., 2021), though no similar studies have looked at the same effect in bivalves this mechanism is still possible. Taken together, these findings could explain the offset between δ^{11}B-based pH and seawater or EPF pH. Nevertheless, this remains speculative as there is no further evidence of boric acid incorporation in these species.

The difference between microelectrode EPF pH and δ^{11}B-based EPF pH implies that pH measured with boron isotopes probes a localized site of calcification rather than the entire EPF pool measured with microelectrode. A spatial and temporal study conducted by Stemmer et al. (2019) measured the EPF of *Arctica islandica* and showed highly dynamic changes in pH, Ca^{2+} and DIC from the surface of the shell to the outer mantle epithelium (OME), with localized environment at the OME reaching pH values up to 9.5. Due to this high variability, it is possible that the EPF microelectrode measurements in this study did not capture the full variability of the EPF. Stemmer et al. (2019) presented EPF pH values measured at the shell surface ranging [7.1-7.6] for *A. islandica*, comparable to the values measured from microelectrode in this study (Fig 9). Additionally, Stemmer et al. (2019) found large influxes of DIC which could not have been explained just from metabolic activity, but instead indicated intense DIC pumping and bursts of calcification. These findings are in line with the holistic view of biomineralization outlined in Checa (2018) and Johnstone (2015) which argue that crystal deposition is a series of periodic events under biological regulation. In our study, a time-series of microelectrode EPF pH shows that at no point, during ventilation and closed cycles, does the EPF pH reach the δ^{11}B-calculated pH (Fig 9). The fact that microelectrode EPF pH is systematically lower than seawater pH for both of our bivalve species may reflect localized differences in pH associated with zones of calcification. The two environments (site of calcification and bulk EPF) can act distinctly, with low pH and high DIC EPF being a source of carbon for the site of calcification in the bulk EPF, and elevated pH of the site of calcification supporting the conversion of the DIC species to $[CO_3^{2-}]$ in support of mineral precipitation. Further work would be needed to assess this highly dynamic and localized environment, however our study shows that boron isotopes may reflect the pH of the microenvironment where calcification occurs within the EPF, which has previously been

inferred by prior studies using non-geochemical approaches (Ramesh et al., 2017; Ramesh et al., 2018; Stemmer et al., 2019).

Conclusion

In this study, we used numerous approaches constraining the geochemical composition of and partitioning between the tripartite reservoirs of the bivalve mineralization system—seawater, EPF and shell. Our study presents Mg/Ca and B/Ca, and absolute Ca^{2+} data of the seawater, EPF and shell. Comparisons of seawater and extrapallial fluid Mg/Ca and B/Ca, Ca^{2+}, and $\delta^{26}Mg$ indicate that the EPF has a distinct composition that differs from seawater. Additionally, our OA experiments show that the EPF Mg/Ca and B/Ca, as well as absolute Mg^{2+}, B, and Ca^{2+}, all were significantly affected by CO_2-induced ocean acidification, demonstrating that the biological pathways regulating or storing these ions involved in calcification are impacted by ocean acidification. Decreased calcium ion concentration within the extrapallial fluid due to OA could impair calcification by lowering the saturation state of the EPF with respect to $CaCO_3$. Additionally, our results show that shell $\delta^{11}B$ does not faithfully record seawater pH. However, shell $\delta^{11}B$ is correlated with EPF pH, despite an offset from *in situ* microelectrode pH measurements. Both microelectrode pH and $\delta^{11}B$-calculated pH decreased with decreasing pH. However, the $\delta^{11}B$-calculated pH values were consistently higher than microelectrode pH measurements, indicating that the shell $\delta^{11}B$ may reflect pH at a more localized site of calcification, rather than pH of the bulk EPF. Furthermore, the offset between the $\delta^{11}B$-calculated pH and microelectrode pH increased with decreasing pH under ocean acidification, indicating OA has a larger effect on bulk pH of the EPF measured via microelectrode than on site of calcification pH—the latter of which the bivalve may have more physiological control over to ensure continued calcification even under chemically unfavorable conditions. These complex dynamics of EPF chemistry suggest that boron proxies in these two bivalve species are not straightforwardly related to seawater pH, precluding utilization of those species for reconstructing the carbonate chemistry of seawater. Moreover, the $\delta^{11}B$ proxy may not be suitable for reconstructing seawater pH for bivalves with high physiological control over their internal calcifying fluid and is further complicated under conditions of moderate and extreme ocean acidification, where $\delta^{11}B$ EPF pH deviates further from bulk microelectrode pH, possibly due to the effect of DIC on shell $\delta^{11}B$ or the tendency for shell $\delta^{11}B$ to reflect EPF pH at the more localized site of calcification, rather than pH of the bulk EPF.

Author contribution

LPC, AD, JBR, and KL designed the experiments and carried them out. BAC, MG, and RAE developed the geochemical study. BAC and MG performed geochemical analysis with the help of JNS and JAH. BAC, MG, and RAE prepared the manuscript with contributions from all co-authors.

Competing interests

The authors declare that they have no conflict of interest.

Acknowledgements

BAC was supported by the National Science Foundation Graduate Research Fellowship Program under Grant No. DGE-2034835 and the UC Eugene Cota-Robles Fellowship. BAC, MG, and RAE are supported by the Ocean Science work of Center for Diverse Leadership in Science which is funded by a grant from the David and Lucile Packard Foundation (no. 85180), National Science Foundation grant NSF-RISE-2024426, and by gifts from Oceankind and Dalio Philanthropies. The Center for Diverse Leadership in Science is also supported by NSF-RISE-2228198, the Waverly Foundation, the Silicon Valley Community Foundation, and the Sloan Foundation. KL and JBR were supported by the National Science Foundation grant BIO-OCE 1635423. The authors would like to thank Celine Liorzou, Yoan Germain, and Anne Trinquier for their technical support at the PSO. Additionally, the authors would like to thank Stefania Gili for her technical support at Princeton University.

References

1. Addadi, L., Raz, S., and Weiner, S.: Taking Advantage of Disorder: Amorphous calcium carbonate and its roles in biomineralization, Advanced Materials, 15, 959–970, 2003.
2. Addadi, L., Joester, D., Nudelman, F., and Weiner, S.: Mollusc Shell Formation: A Source of New Concepts for Understanding Biomineralization Processes, Chemistry A European J, 12, 980–987, 2006.
3. Ahm, A.-S. C., Bjerrum, C. J., Hoffman, P. F., Macdonald, F. A., Maloof, A. C., Rose, C. V., Strauss, J. V., and Higgins, J. A.: The Ca and Mg isotope record of the Cryogenian Trezona carbon isotope excursion, Earth and Planetary Science Letters, 568, 117002, 2021.
4. Alibert, C. and McCulloch, M. T.: Strontium/calcium ratios in modern *porites* corals From the Great Barrier Reef as a proxy for sea surface temperature: Calibration of the thermometer and monitoring of ENSO, Paleoceanography, 12, 345–363, 1997.
5. Allison, N. and Finch, A. A.: δ^{11}B, Sr, Mg and B in a modern Porites coral: the relationship between calcification site pH and skeletal chemistry, Geochimica et Cosmochimica Acta, 74, 1790–1800, 2010.
6. Barker, S., Greaves, M., and Elderfield, H.: A study of cleaning procedures used for foraminiferal Mg/Ca paleothermometry, Geochemistry, Geophysics, Geosystems, 4(9), 2003.

7. Beniash, E., Ivanina, A., Lieb, N. S., Kurochkin, I., and Sokolova, I. M.: Elevated level of carbon dioxide affects metabolism and shell formation in oysters *Crassostrea virginica*, Marine Ecology Progress Series, 419, 95–108, 2010.
8. Broecker, W. S. and Peng, T.-H.: Tracers in the Sea, Lamont-Doherty Geological Observatory, Columbia University Palisades, New York, 1982.
9. Cameron, L. P., Understanding Patterns of Bivalve Vulnerability and Resilience to Ocean Acidification: Insights from Field Studies, Tank Experiments and Novel Physiological Studies, Dissertation Northeastern University, 2020.
10. Cameron, L.P., Reymond, C.E., Bijma, J., Büscher, J.V., de Beer, D., Guillermic, M., Eagle, R.A., Gunnell, J., Müller-Lundin, F., Schmidt-Grieb, G.M., Westfield, I., Westphal, H., Ries, J.B., Impacts of warming and acidification on coral calcification linked to photosymbiont loss and deregulation of calcifying fluid pH, Journal of Marine Science and Engineering, 10, 1106, 2022.
11. Cameron, L. P., Grabowski, J. H., Ries, J. B., Impact of ocean acidification and warming on calcification rate, survival, extrapallial fluid chemistry, and respiration of the Atlantic sea scallop Placopecten magellanicus, Limnology & Oceanography, 1-17, 2019.
12. Checa, A. G.: Physical and Biological Determinants of the Fabrication of Molluscan Shell Microstructures, Frontiers in Marine Science, 5, 2018.
13. Cornwall, C. E., Comeau, S., and McCulloch, M. T.: Coralline algae elevate pH at the site of calcification under ocean acidification, Global Change Biology, 23, 4245–4256, 2017.
14. Craig, H.: The geochemistry of the stable carbon isotopes, Geochimica et cosmochimica acta, 3, 53–92, 1953.
15. Crenshaw, M. A.: The inorganic composition of molluscan extrapallial fluid, The Biological Bulletin, 143, 506–512, 1972.
16. Cusack, M., Kamenos, N. A., Rollion-Bard, C., and Tricot, G.: Red coralline algae assessed as marine pH proxies using 11B MAS NMR, Scientific Reports, 5, 8175, 2015.
17. Downey-Wall, A. M., Cameron, L. P., Ford, B. M., McNally, E. M., Venkataraman, Y. R., Roberts, S. B., Ries, J. B., and Lotterhos, K. E.: Ocean acidification induces subtle shifts in gene expression and DNA methylation in mantle tissue of the Eastern oyster (*Crassostrea virginica*), Frontiers in Marine Science, 7, 566419, 2020.
18. Dunbar, R. B., Wellington, G. M., Colgan, M. W., and Glynn, P. W.: Eastern Pacific sea surface temperature since 1600 A.D.: The $\delta^{18}O$ record of climate variability in Galápagos Corals, Paleoceanography, 9, 291–315, 1994.
19. Eagle, R. A., Guillermic, M., De Corte, I., Alvarez Caraveo, B., Bove, C. B., Misra, S., Cameron, L. P., Castillo, K. D., and Ries, J. B.: Physicochemical Control of Caribbean Coral Calcification Linked to Host and Symbiont Responses to Varying pCO_2 and Temperature, Journal of Marine Science and Engineering, 10, 1075, 2022.
20. Elderfield, H., Yu, J., Anand, P., Kiefer, T., and Nyland, B.: Calibrations for benthic foraminiferal Mg/Ca paleothermometry and the carbonate ion hypothesis, Earth and Planetary Science Letters, 250, 633–649, 2006.

21. Fitzer, S. C., Chung, P., Maccherozzi, F., Dhesi, S. S., Kamenos, N. A., Phoenix, V. R., and Cusack, M.: Biomineral shell formation under ocean acidification: a shift from order to chaos, Scientific Reports, 6, 21076, 2016.
22. Foster, G. L. and Rae, J. W. B.: Reconstructing Ocean pH with Boron Isotopes in Foraminifera, Annual Review of Earth and Planetary Sciences, 44, 207–237, 2016.
23. Gagnon, A. C., Gothmann, A. M., Branson, O., Rae, J. W. B., and Stewart, J. A.: Controls on boron isotopes in a cold-water coral and the cost of resilience to ocean acidification, Earth and Planetary Science Letters, 554, 116662, 2021.
24. Gaillardet, J., Lemarchand, D., Göpel, C., and Manhès, G.: Evaporation and Sublimation of Boric Acid: Application for Boron Purification from Organic Rich Solutions, Geostandards Newsletter, 25, 67–75, 2001.
25. Gazeau, F., Parker, L. M., Comeau, S., Gattuso, J.-P., O'Connor, W. A., Martin, S., Pörtner, H.-O., and Ross, P. M.: Impacts of ocean acidification on marine shelled molluscs, Marine Biology, 160, 2207–2245, 2013.
26. Gibson, R., Barnes, M., and Atkinson, R.: Molluscs as archives of environmental change, Oceanography Marine Biology Annual Review, 39, 103–164, 2001.
27. Gilbert, P., Bergmann, K. D., Boekelheide, N., Tambutté, S., Mass, T., Marin, F., Adkins, J. F., Erez, J., Gilbert, B., Knutson, V., Cantine, M., Hernández, J. O., and Knoll, A. H.: Biomineralization: Integrating mechanism and evolutionary history, Science Advances, 8, eabl9653, 2022.
28. Gosling, E.: Bivalve molluscs: biology, ecology and culture, John Wiley & Sons, 2008.
29. Guillermic, M., Cameron, L. P., De Corte, I., Misra, S., Bijma, J., De Beer, D., Reymond, C. E., Westphal, H., Ries, J. B., and Eagle, R. A.: Thermal stress reduces pocilloporid coral resilience to ocean acidification by impairing control over calcifying fluid chemistry, Science Advances, 7, eaba9958, 2021.
30. Gutjahr, M., Bordier, L., Douville, E., Farmer, J., Foster, G. L., Hathorne, E. C., Hönisch, B., Lemarchand, D., Louvat, P., McCulloch, M., Noireaux, J., Pallavicini, N., Rae, J. W. B., Rodushkin, I., Roux, P., Stewart, J. A., Thil, F., and You, C.: Sub-Permil Interlaboratory Consistency for Solution-Based Boron Isotope Analyses on Marine Carbonates, Geostandards and Geoanalytical Research, 45, 59–75, 2021.
31. Heinemann, A., Fietzke, J., Melzner, F., Böhm, F., Thomsen, J., Garbe-Schönberg, D., and Eisenhauer, A.: Conditions of Mytilus edulis extracellular body fluids and shell composition in a pH-treatment experiment: Acid-base status, trace elements and $\delta^{11}B$, Geochemistry Geophysics Geosystems, 13, 2011GC003790, 2012.
32. Helm, M. M., Bourne, N., and Lovatelli, A.: Hatchery culture of bivalves: a practical manual, 2004.
33. Hemming, N. G. and Hanson, G. N.: Boron isotopic composition and concentration in modern marine carbonates, Geochimica et Cosmochimica Acta, 56, 537–543, 1992.
34. Hess, P., Lansman, J. B., & Tsien, R. W. Calcium channel selectivity for divalent and monovalent cations. Voltage and concentration dependence of single channel current in ventricular heart cells. The Journal of general physiology, 88(3), 293-319, 1986.

35. Higgins, J. A., Blättler, C. L., Lundstrom, E. A., Santiago-Ramos, D. P., Akhtar, A. A., Crüger Ahm, A.-S., Bialik, O., Holmden, C., Bradbury, H., Murray, S. T., and Swart, P. K.: Mineralogy, early marine diagenesis, and the chemistry of shallow-water carbonate sediments, Geochimica et Cosmochimica Acta, 220, 512–534, 2018.
36. Hönisch, B., Hemming, Ng., Grottoli, A. G., Amat, A., Hanson, G. N., and Bijma, J.: Assessing scleractinian corals as recorders for paleo-pH: Empirical calibration and vital effects, Geochimica et Cosmochimica Acta, 68, 3675–3685, 2004.
37. Husson, J. M., Higgins, J. A., Maloof, A. C., and Schoene, B.: Ca and Mg isotope constraints on the origin of Earth's deepest $\delta^{13}C$ excursion, Geochimica et Cosmochimica Acta, 160, 243–266, 2015.
38. Immenhauser, A., Schöne, B. R., Hoffmann, R., and Niedermayr, A.: Mollusc and brachiopod skeletal hard parts: Intricate archives of their marine environment, Sedimentology, 63, 1–59, 2016.
39. Johnstone, M. B., Gohad, N. V., Falwell, E. P., Hansen, D. C., Hansen, K. M., and Mount, A. S.: Cellular orchestrated biomineralization of crystalline composites on implant surfaces by the eastern oyster, *Crassostrea virginica* (Gmelin, 1791), Journal of Experimental Marine Biology and Ecology, 463, 8–16, 2015.
40. Klochko, K., Kaufman, A. J., Yao, W., Byrne, R. H., and Tossell, J. A.: Experimental measurement of boron isotope fractionation in seawater, Earth and Planetary Science Letters, 248, 276–285, 2006.
41. Klochko, K., Cody, G. D., Tossell, J. A., Dera, P., & Kaufman, A. J. Re-evaluating boron speciation in biogenic calcite and aragonite using 11B MAS NMR. Geochimica et Cosmochimica Acta, 73(7), 1890-1900, 2009.
42. Kroeker, K. J., Micheli, F., Gambi, M. C., & Martz, T. R. Divergent ecosystem responses within a benthic marine community to ocean acidification. Proceedings of the National Academy of Sciences, 108(35), 14515-14520, 2011.
43. Liu, Y.-W., Sutton, J. N., Ries, J. B., and Eagle, R. A.: Regulation of calcification site pH is a polyphyletic but not always governing response to ocean acidification, Science Advances, 6, eaax1314, 2020.
44. Liu, Y.-W., Wanamaker Jr, A. D., Aciego, S. M., Searles, I., Hangstad, T. A., Chierici, M., and Carroll, M. L.: Resistant calcification responses of *Arctica islandica* clams under ocean acidification conditions, Journal of Experimental Marine Biology and Ecology, 560, 151855, 2023.
45. Lorens, R. B. and Bender, M. L.: Physiological exclusion of magnesium from *Mytilus edulis* calcite, Nature, 269, 793–794, 1977.
46. Mavromatis, V., Gautier, Q., Bosc, O., & Schott, J. Kinetics of Mg partition and Mg stable isotope fractionation during its incorporation in calcite. Geochimica et Cosmochimica Acta, 114, 188-203, 2013
47. McCulloch, M. T., D'Olivo, J. P., Falter, J., Holcomb, M., and Trotter, J. A.: Coral calcification in a changing world and the interactive dynamics of pH and DIC upregulation, Nature Communications, 8, 15686, 2017.
48. McCulloch, M. T., D'Olivo, J. P., Falter, J., Georgiou, L., Holcomb, M., Montagna, P., and Trotter, J. A.: Boron Isotopic Systematics in Scleractinian Corals and the Role of pH Up-regulation, in: Boron Isotopes, Springer International Publishing, Cham, 145–162, 2018.

49. McNally, E. M., Downey-Wall, A. M., Titmuss, F. D., Cortina, C., Lotterhos, K., and Ries, J. B.: Parental exposure of Eastern oysters (*Crassostrea virginica*) to elevated p CO 2 mitigates its negative effects on early larval shell growth and morphology, Limnology & Oceanography, 67, 1732–1745, 2022.
50. Michaelidis, B., Ouzounis, C., Paleras, A., and Pörtner, H. O.: Effects of long-term moderate hypercapnia on acid–base balance and growth rate in marine mussels Mytilus galloprovincialis, Marine Ecology Progress Series, 293, 109–118, 2005.
51. Mount, A. S., Wheeler, A. P., Paradkar, R. P., and Snider, D.: Hemocyte-Mediated Shell Mineralization in the Eastern Oyster, Science, 304, 297–300, 2004.
52. Nir, O., Vengosh, A., Harkness, J. S., Dwyer, G. S., and Lahav, O.: Direct measurement of the boron isotope fractionation factor: Reducing the uncertainty in reconstructing ocean paleo-pH, Earth and Planetary Science Letters, 414, 1–5, 2015.
53. Norrie, C. R., Dunphy, B. J., Ragg, N. L. C., & Lundquist, C. J. Ocean acidification can interact with ontogeny to determine the trace element composition of bivalve shell. Limnology and Oceanography Letters, 3(5), 393-400, 2018.
54. Orr, J. C., Fabry, V. J., Aumont, O., Bopp, L., Doney, S. C., Feely, R. A., ... & Yool, A. Anthropogenic ocean acidification over the twenty-first century and its impact on calcifying organisms. Nature, 437(7059), 681-686, 2005
55. Peharda, M., Schöne, B. R., Black, B. A., and Correge, T.: Advances of sclerochronology research in the last decade, Palaeogeography, Palaeoclimatology, Palaeoecology, 570, 110371, 2021.
56. Pierrot, D. E., Wallace, D. W. R., and Lewis, E.: MS Excel program developed for CO2 system calculations, Carbon dioxide information analysis center, 2011.
57. Planchon, F., Poulain, C., Langlet, D., Paulet, Y.-M., and André, L.: Mg-isotopic fractionation in the manila clam (*Ruditapes philippinarum*): New insights into Mg incorporation pathway and calcification process of bivalves, Geochimica et cosmochimica acta, 121, 374–397, 2013.
58. Raitzsch, M., Bijma, J., Bickert, T., Schulz, M., Holbourn, A., & Kučera, M. (2021). Atmospheric carbon dioxide variations across the middle Miocene climate transition. Climate of the Past, 17(2), 703-719.
59. Ramesh, K., Hu, M. Y., Thomsen, J., Bleich, M., & Melzner, F. Mussel larvae modify calcifying fluid carbonate chemistry to promote calcification. Nature Communications, 8(1), 1709, 2017.
60. Ramesh, K., Melzner, F., Griffith, A. W., Gobler, C. J., Rouger, C., Tasdemir, D., and Nehrke, G.: In vivo characterization of bivalve larval shells: a confocal Raman microscopy study, Journal of the Royal Society Interface,, 15, 20170723, 2018.
61. Ries, J. B., Cohen, A. L., and McCorkle, D. C.: Marine calcifiers exhibit mixed responses to CO_2-induced ocean acidification, Geology, 37, 1131–1134, 2009.

62. Ries, J. B., Ghazaleh, M. N., Connolly, B., Westfield, I., and Castillo, K. D.: Impacts of seawater saturation state (ØmegaA= 0.4–4.6) and temperature (10, 25 C) on the dissolution kinetics of whole-shell biogenic carbonates, Geochimica et Cosmochimica Acta, 192, 318–337, 2016.
63. Rollion-Bard, C., Blamart, D., Trebosc, J., Tricot, G., Mussi, A., and Cuif, J.-P.: Boron isotopes as pH proxy: A new look at boron speciation in deep-sea corals using ^{11}B MAS NMR and EELS, Geochimica et cosmochimica acta, 75, 1003–1012, 2011.
64. Sanyal, A., Bijma, J., Spero, H., and Lea, D. W.: Empirical relationship between pH and the boron isotopic composition of *Globigerinoides sacculifer* : Implications for the boron isotope paleo-pH proxy, Paleoceanography, 16, 515–519, 2001.
65. Saulnier, S., Rollion-Bard, C., Vigier, N., and Chaussidon, M.: Mg isotope fractionation during calcite precipitation: An experimental study, Geochimica et Cosmochimica Acta, 91, 75–91, 2012.
66. Schöne, B. R., Zhang, Z., Radermacher, P., Thébault, J., Jacob, D. E., Nunn, E. V., & Maurer, A. F. Sr/Ca and Mg/Ca ratios of ontogenetically old, long-lived bivalve shells (*Arctica islandica*) and their function as paleotemperature proxies. Palaeogeography, palaeoclimatology, palaeoecology, 302(1-2), 52-64, 2011.
67. Sillanpää, J. K., Ramesh, K., Melzner, F., Sundh, H., and Sundell, K.: Calcium mobilisation following shell damage in the Pacific oyster, *Crassostrea gigas*, Marine Genomics, 27, 75–83, 2016.
68. Sillanpää, J. K., Sundh, H., and Sundell, K. S.: Calcium transfer across the outer mantle epithelium in the Pacific oyster, *Crassostrea gigas*, Proceedings of the Royal Society B: Biological Sciences, 285, 20181676, 2018.
69. Sillanpää, J. K., Cardoso, J. C. dos R., Félix, R. C., Anjos, L., Power, D. M., and Sundell, K.: Dilution of seawater affects the Ca^{2+} transport in the outer mantle epithelium of *Crassostrea gigas*, Frontiers in Physiology, 11, 496427, 2020.
70. Stemmer, K., Brey, T., Gutbrod, M. S., Beutler, M., Schalkhausser, B., and De Beer, D.: In situ measurements of pH, Ca^{2+}, and DIC dynamics within the extrapallial fluid of the ocean quahog *Arctica islandica*, Journal of Shellfish Research, 38, 71–78, 2019.
71. Stewart-Sinclair, P. J., Last, K. S., Payne, B. L., and Wilding, T. A.: A global assessment of the vulnerability of shellfish aquaculture to climate change and ocean acidification, Ecology and Evolution, 10, 3518–3534, 2020.
72. Stoll, H., Langer, G., Shimizu, N., and Kanamaru, K.: B/Ca in coccoliths and relationship to calcification vesicle pH and dissolved inorganic carbon concentrations, Geochimica et cosmochimica acta, 80, 143–157, 2012.
73. Sutton, J. N., Liu, Y.-W., Ries, J. B., Guillermic, M., Ponzevera, E., and Eagle, R. A.: δ^{11}B as monitor of calcification site pH in divergent marine calcifying organisms, Biogeosciences, 15, 1447–1467, 2018.
74. Thomsen, J., Casties, I., Pansch, C., Körtzinger, A., and Melzner, F.: Food availability outweighs ocean acidification effects in juvenile *Mytilus edulis* : laboratory and field experiments, Global Change Biology, 19, 1017–1027, 2013.

75. Ulrich, R. N., Guillermic, M., Campbell, J., Hakim, A., Han, R., Singh, S., Stewart, J. D., Román-Palacios, C., Carroll, H. M., and De Corte, I.: Patterns of element incorporation in calcium carbonate biominerals recapitulate phylogeny for a diverse range of marine calcifiers, Frontiers in earth science, 9, 641760, 2021.
76. Urey, H. C., Lowenstam, H. A., Epstein, S., and McKinney, C. R.: Measurement of paleotemperatures and temperatures of the Upper Cretaceous of England, Denmark, and the southeastern United States, Geological Society of America Bulletin, 62, 399–416, 1951.
77. Vogl, J., Rosner, M., and Pritzkow, W.: Development and validation of a single collector SF-ICPMS procedure for the determination of boron isotope ratios in water and food samples, Journal of analytical atomic spectrometry, 26, 861–869, 2011.
78. Waldbusser, G. G., Voigt, E. P., Bergschneider, H., Green, M. A., and Newell, R. I. E.: Biocalcification in the Eastern Oyster (*Crassostrea virginica*) in Relation to Long-term Trends in Chesapeake Bay pH, Estuaries and Coasts, 34, 221–231, 2011.
79. Waldbusser, G. G., Hales, B., Langdon, C. J., Haley, B. A., Schrader, P., Brunner, E. L., ... & Gimenez, I. Saturation-state sensitivity of marine bivalve larvae to ocean acidification. Nature Climate Change, 5(3), 273-280, 2015.
80. Wanamaker Jr, A. D., Kreutz, K. J., Wilson, T., Borns Jr, H. W., Introne, D. S., and Feindel, S.: Experimentally determined Mg/Ca and Sr/Ca ratios in juvenile bivalve calcite for *Mytilus edulis*: implications for paleotemperature reconstructions, Geo-Marine Letters, 28, 359–368, 2008.
81. Wang, B.-S., You, C.-F., Huang, K.-F., Wu, S.-F., Aggarwal, S. K., Chung, C.-H., and Lin, P.-Y.: Direct separation of boron from Na-and Ca-rich matrices by sublimation for stable isotope measurement by MC-ICP-MS, Talanta, 82, 1378–1384, 2010.
82. Wang, X., Wang, M., Jia, Z., Qiu, L., Wang, L., Zhang, A., and Song, L.: A Carbonic Anhydrase Serves as an Important Acid-Base Regulator in Pacific Oyster Crassostrea gigas Exposed to Elevated CO_2: Implication for Physiological Responses of mollusc to Ocean Acidification, Marine Biotechnology, 19, 22–35, 2017.
83. Weiner, S., & Dove, P. M. . An overview of biomineralization processes and the problem of the vital effect. Reviews in mineralogy and geochemistry, 54(1), 1-29, 2003.
84. Wilbur, K. M., & Saleuddin, A. S. M. Shell formation. In The mollusca (pp. 235-287). Academic Press, 1983.
85. Wilbur, K. M. and Bernhardt, A. M.: Effects of amino acids, magnesium, and molluscan extrapallial fluid on crystallization of calcium carbonate: In vitro experiments, The Biological Bulletin, 166, 251–259, 1984.
86. Zeebe, R. E. and Wolf-Gladrow, D.: CO_2 in Seawater: Equilibrium, Kinetics, Isotopes, Gulf Professional Publishing, 382 pp., 2001.
87. Zhao, L., Milano, S., Walliser, E. O., and Schöne, B. R. Bivalve shell formation in a naturally CO_2-enriched habitat: Unraveling the resilience mechanisms from elemental signatures, Chemosphere, 203, 132–138, 2018.

88. Zhao, L., Milano, S., Tanaka, K., Liang, J., Deng, Y., Yang, F., Walliser, E.O., and Schöne, B. R. Trace elemental alterations of bivalve shells following transgenerational exposure to ocean acidification: Implications for geographical traceability and environmental reconstruction. Science of the Total Environment, 705, 135501, 2020.
89. Zittier, Z. M., Bock, C., Lannig, G., and Pörtner, H. O.: Impact of ocean acidification on thermal tolerance and acid–base regulation of *Mytilus edulis* (L.) from the North Sea, Journal of experimental marine biology and ecology, 473, 16–25, 2015.